



TECHNISCHE
UNIVERSITÄT
WIEN

Vienna University of Technology
Faculty of Technical Chemistry
Institute for Applied Synthetic Chemistry
Institute for Chemical Technologies and Analytics



www.thvt.at

Experimental and in-silico characterization of microfluidic concentration gradient generators

MASTER THESIS

Author: Mhammad Mayassa

First Supervisor: Univ. Prof. Dipl.- Ing. Dr. Peter Ertl

Second Supervisor: Ass. Prof. Dipl.- Ing. Dr. Michael Harasek

December 2018, Vienna

TABLE OF CONTENT

LIST OF FIGURES	-----	3
LIST OF TABLES	-----	5
1	ABSTRACT	----- 6
2	INTRODUCTION	----- 7
2.1	Definition of Microfluidics	----- 7
2.1.1	Key application areas of microfluidics	----- 7
2.2	Microfluidic gradient generators	----- 10
2.2.1	Types of microfluidic gradient generator designs	----- 10
2.3	Fluid Mechanics in Microfluidic channels	----- 13
2.3.1	Transport Phenomena	----- 13
2.3.2	Navier-Stokes equation	----- 13
2.3.3	Reynolds Number	----- 14
2.3.4	Hagen-Poiseuille's law	----- 17
2.3.5	Hydraulic Resistance	----- 17
2.3.6	Mixing phenomena	----- 20
3	GOALS OF THE THESIS	----- 24
4	MATERIALS AND METHODS	----- 25
4.1	Photomask design using AutoCAD	----- 25
4.2	Fabrication of master mold by photolithography	----- 25
4.2.1	Fabrication tools	----- 25
4.2.2	Fabrication procedure	----- 26
4.3	Fabrication of the gradient generator using OSTEMER	----- 27
4.3.1	Fabrication tools	----- 27
4.3.2	Fabrication procedure	----- 28
4.4	Fabrication of microfluidic gradient generator by using PDMS	----- 29
4.4.1	Fabrication tools	----- 29
4.4.2	Fabrication procedure	----- 31
4.5	Evaluation of the microfluidic gradient generator	----- 31
4.5.1	Experimental set-up tools	----- 31
4.5.2	Set-up procedure	----- 33
4.5.3	Gravimetric evaluation of microfluidic gradient generator	----- 34
4.5.4	Spectroscopic evaluation of the microfluidic gradient generator	----- 35

4.6	Simulation of the microfluidic gradient generator -----	39
4.6.1	Computational fluid dynamics:-----	39
4.6.2	Simulation process:-----	39
4.6.3	GAMBIT-----	40
4.6.4	Fluent-----	43
5	RESULTS AND DISCUSSION -----	48
5.1	Gravimetric results-----	48
5.2	On-chip Generation of Fluorescein Sodium Salt-----	59
5.3	Simulation Results for Fluorescein Sodium Salt -----	60
5.4	Comparison between experimental and CFD simulation for concentration gradient generator chips	63
6	CONCLUSION -----	67
7	REFERENCES -----	68

LIST OF FIGURES

Figure 1: PDMS-based microfluidic gradient generator.	8
Figure 2: Schematic images of a lab-on-chip device [11], [12].	8
Figure 3: a Microfluidic chemostat study the growth of microbial populations, integrated with pneumatic valves [1].	9
Figure 4: Schematic of Micro mosaic Immunoassay preparation and its multiple stages: a) immobilization, b) blocking, c) recognition, d) reading mosaic [13].	9
Figure 5: Y-shape microfluidic gradient generator [18].	11
Figure 6: Multi-layer concentration gradient generator of membrane systems [18]	11
Figure 7: Single layer microfluidic pressure balance gradient generator [18]	12
Figure 8: Droplet generation microfluidic system to gain molecular gradients [18].	13
Figure 9: Laminar flow versus turbulent flow and the Reynolds number [34].	16
Figure 10: Similarity between electric circuit and hydraulic circuit [14].	19
Figure 11: Schematic (upper panel) and technical drawing (lower panel) of the microfluidic gradient generator including channel and chip dimensions using AutoCAD.	25
Figure 12: Master Mold fabrication tools: a) Laminator. b) Exposure masking system. c) Heating plate. d) Plasma cleaner. e) Oven. d) Nitrogen guns.	26
Figure 13: Fabrication of the gradient generator using OSTEMER tools. a) Analytical balance. b) Vortex. c) Degasser. d) Oven.	28
Figure 14: OSTEMER two components.	29
Figure 15: PDMS structure [44].	30
Figure 16: Silicone elastomer and its curing agent.	30
Figure 17: Experimental setup tools: a) microfluidic gradient generator chip. b) syringe pump. c) microscopy. d) two syringes. e) Tygon tubes. f) Eppendorf tubes	32
Figure 18: Fluorescein structure.	33
Figure 19: Boxing diagram of the set-up.	33
Figure 20: Experimental set-up.	34
Figure 21: Gravimetric measurement tools: a) Analytical Balance, b) Pipette, c) Pipette tips, d) Eppendorf tubes	35
Figure 22: Spectroscopic measurement tools: a) multimode plate reader, b) pipette, c) microplate, d) Eppendorf tubes	36
Figure 23: Calibration curve. Y: fluorescein intensity, X: fluorescein concentration	37
Figure 24: Gambit interface and GUI components.	40
Figure 25: Random geometry as an example	41
Figure 26: specify boundary types.	42
Figure 27: 3-D meshed geometry in Gambit.	43
Figure 28: Length unit scaling	44
Figure 29: fluorescein and liquid water mixture define	45
Figure 30: Boundary conditions define.	46
Figure 31: Discretization settings	47
Figure 32: Residual and surface monitors.	48
Figure 33: a) The liquid compound weights at every outlet for (30 μm) height chip at a flow rate (100 $\mu\text{l}/\text{min}$). b) The liquid compound weights at every outlet for (30 μm) height chip at a flow rate (80 $\mu\text{l}/\text{min}$). c) The liquid compound weights at every outlet for	

(30 μm) height chip at a flow rate (60 $\mu\text{l}/\text{min}$). d) The liquid compound weights at every outlet for (30 μm) height chip at a flow rate (40 $\mu\text{l}/\text{min}$).	50
Figure 34: a) The liquid compound weights at every outlet for (30 μm) height chip at a flow rate (20 $\mu\text{l}/\text{min}$). b) The liquid compound weights at every outlet for (30 μm) height chip at a flow rate (10 $\mu\text{l}/\text{min}$). c) The liquid compound weights at every outlet for (30 μm) height chip at a flow rate (5 $\mu\text{l}/\text{min}$).....	51
Figure 35: a) The liquid compound weights at every outlet for (30 μm) height chip at a flow rate (1 $\mu\text{l}/\text{min}$). b) The liquid compound weights at every outlet for (30 μm) height chip at a flow rate (0.5 $\mu\text{l}/\text{min}$).	51
Figure 36: Comparison of the liquid compound total weight at each different flow rate of (30 μm) height chip.	52
Figure 37: a) The liquid compound weights at every outlet for (45 μm) height chip at a flow rate (100 $\mu\text{l}/\text{min}$). b) The liquid compound weights at every outlet for (45 μm) height chip at a flow rate (80 $\mu\text{l}/\text{min}$). c) The liquid compound weights at every outlet for (45 μm) height chip at a flow rate (60 $\mu\text{l}/\text{min}$). d) The liquid compound weights at every outlet for (45 μm) height chip at a flow rate (40 $\mu\text{l}/\text{min}$).	53
Figure 38: a) The liquid compound weights at every outlet for (45 μm) height chip at a flow rate (20 $\mu\text{l}/\text{min}$). b) The liquid compound weights at every outlet for (45 μm) height chip at a flow rate (10 $\mu\text{l}/\text{min}$). c) The liquid compound weights at every outlet for (45 μm) height chip at a flow rate (5 $\mu\text{l}/\text{min}$).....	54
Figure 39: a) The liquid compound weights at every outlet for (45 μm) height chip at a flow rate (1 $\mu\text{l}/\text{min}$). b) The liquid compound weights at every outlet for (45 μm) height chip at a flow rate (0,5 $\mu\text{l}/\text{min}$).	54
Figure 40: Comparison of the liquid compound total weight at each different flow rate of (45 μm) height chip.	55
Figure 41: a) The liquid compound weights at every outlet for (90 μm) height chip at flow rate (100 $\mu\text{l}/\text{min}$). b) The liquid compound weights at every outlet for (90 μm) height chip at flow rate (80 $\mu\text{l}/\text{min}$). c) The liquid compound weights at every outlet for (90 μm) height chip at flow rate (60 $\mu\text{l}/\text{min}$). d) The liquid compound weights at every outlet for (90 μm) height chip at flow rate (40 $\mu\text{l}/\text{min}$).....	56
Figure 42: a) The liquid compound weights at every outlet for (90 μm) height chip at a flow rate (20 $\mu\text{l}/\text{min}$). b) The liquid compound weights at every outlet for (90 μm) height chip at a flow rate (10 $\mu\text{l}/\text{min}$). c) The liquid compound weights at every outlet for (90 μm) height chip at a flow rate (5 $\mu\text{l}/\text{min}$).....	57
Figure 43: a) The liquid compound weights at every outlet for (90 μm) height chip at a flow rate (1 $\mu\text{l}/\text{min}$). b) The liquid compound weights at every outlet for (90 μm) height chip at a flow rate (0,5 $\mu\text{l}/\text{min}$).	57
Figure 44: Comparison of the liquid compound total weight at each different flow rate of (90 μm) height chip.	58
Figure 45: (a-i) Comparison between experimental data and CFD simulation results for 100 $\mu\text{g}/\text{ml}$ fluorescein sodium salt solution for 30 μm high microfluidic gradient generators.	64
Figure 46: (a-i) Comparison between experimental data and CFD simulation results for 100 $\mu\text{g}/\text{ml}$ fluorescein sodium salt solution for 45 μm high microfluidic gradient generators.	65

Figure 47: (a-i) Comparison between experimental data and CFD simulation results for 100 µg/ml fluorescein sodium salt solution for 90 µm high microfluidic gradient generators. 66

LIST OF TABLES

Table 1: Similarity between electric and hydraulic circuit.	18
Table 2: Fluorescein intensities results	37
Table 3: fluorescein intensity values of (30 µm) height chip.	38
Table 4: fluorescein intensity values of (45 µm) height chip.	38
Table 5: fluorescein intensity values of (90 µm) height chip.	38
Table 6: velocities through the inlets for different flow rates and different chips heights.	46
Table 7: Gravimetric results of the (30 µm) height chip.....	48
Table 8: Gravimetric results of the (45 µm) height chip.....	52
Table 9: Gravimetric results of the (90 µm) chip.	55
Table 10: Experiment Fluorescein concentration results at different flow rates of (30 µm) height chip.	59
Table 11: Experiment Fluorescein concentration results at different flow rates of (45 µm) height chip.	59
Table 12: Experiment Fluorescein concentration results at different flow rates of (90 µm) height chip.	60
Table 13: Simulation Fluorescein concentration results at different flow rates of (30 µm) height chip.	60
Table 14: Simulation Fluorescein concentration results at different flow rates of (45 µm) height chip.	61
Table 15: Simulation Fluorescein concentration results at different flow rates of (90 µm) height chip.	61
Table 16: Simulation Fluorescein concentration results at different flow rates of (250 µm) height chip.	62
Table 17: Simulation Fluorescein concentration results at different flow rates of (500 µm) height chip.	62

1 ABSTRACT

Due to importance of gradients in chemistry and biology, stable and controllable gradient concentrations in microfluidics has significance for analysis of cell migration, cancer metastasis, drug screening, chemotaxis as well as chemical synthesis and mixing. Microfluidic devices offer the possibility of generating complex and well-defined gradient profiles. Fluid streams at the micron scale can provide a tool to recreate and control these gradients over space and time. Furthermore, besides advantages like deterministic flow (i.e. low Reynolds number), reduced costs and ease of manufacturing, microfluidics gives the possibility to observe cell-related processes at the same scale at which they take place. One of the most popular methods for generating chemical gradients is to leverage the tree-shaped design, where two or more fluids are mixed in different ratios by a channel network, forming a gradient in the main channel by laminar flow. Because of the laminar regime that is inherent to fluid flow in microchannels, the geometry of the microdevice and the flow rates can be tuned to subject for instance cultured cells to well-defined concentration profiles. In this thesis, a diffusion-dependent microfluidic concentration gradient generator was designed and fabricated using the photo – and soft lithography. Three different channel heights were produced (30 μm , 45 μm , 90 μm) and tested at different flow rates (100 $\mu\text{L}/\text{min}$ - 0.5 $\mu\text{L}/\text{min}$). Concentration gradient splitting and fluid dynamics were simulated using Computational Fluid Dynamic (CFD) simulation tools (Gambit and Fluent) for the three different channel heights at different flow rates. These results were compared to experimental, gravimetric and spectroscopic measurements to evaluate the chip performance and the best operating range with respect to flow rate.

2 INTRODUCTION

2.1 DEFINITION OF MICROFLUIDICS

Microfluidics is the science and technology which studies the behavior, the act and the manipulation of fluids varying from microliters to femtoliters in micrometer scaled channels [1]. Microfluidic devices have many advantages such as low sample and reagent consumption, and the precise control of gradients and concentrations. Such devices are often portable and allow the fabrication at relatively low cost, parallelization and high throughput sample analysis [2] as well as high resolution and sensitivity detection [1], [3]. All these advantages make it a multidisciplinary science at the intersection of physics, chemistry, engineering, and optics. Microfluidic systems are known for its applications for immunoassays[4], DNA analysis [5], flow cytometry [6], capillary electrophoresis [7], PCR amplification [8], cell separation [9]and cell patterning [10]. The earliest microanalytical methods included capillary electrophoresis (CE), gas-phase chromatography (GPC) [1].

2.1.1 Key application areas of microfluidics

2.1.1.1 Microfluidic gradient generators

Application of microfluidic systems abroad and range from a simple linear channel for the cultivation of mammalian cell cultures as well as highly integrated and automated lab-on-a-chip systems to micro physiological systems that aim for recreation of human physiology and organ function on a chip-based platform.

For instance microfluidic gradient generators provide the tools to recreate and control molecular gradients over space and time. Figure 1 shows the microfluidic tree -shaped gradient generator, which will be discussed also later in the thesis, where chemical or biochemical gradients are generated by exploiting the separation and conjunction of two or more liquid streams due to laminar flow and diffusion. Microfluidic gradient generators are often integrated within lab-on-a-chip systems as one of many on-chip functions that automate and miniaturize bioassays on a single chip-based platform. Microfluidic gradient generators will be discussed in more detail in Section 2.2 of this thesis.

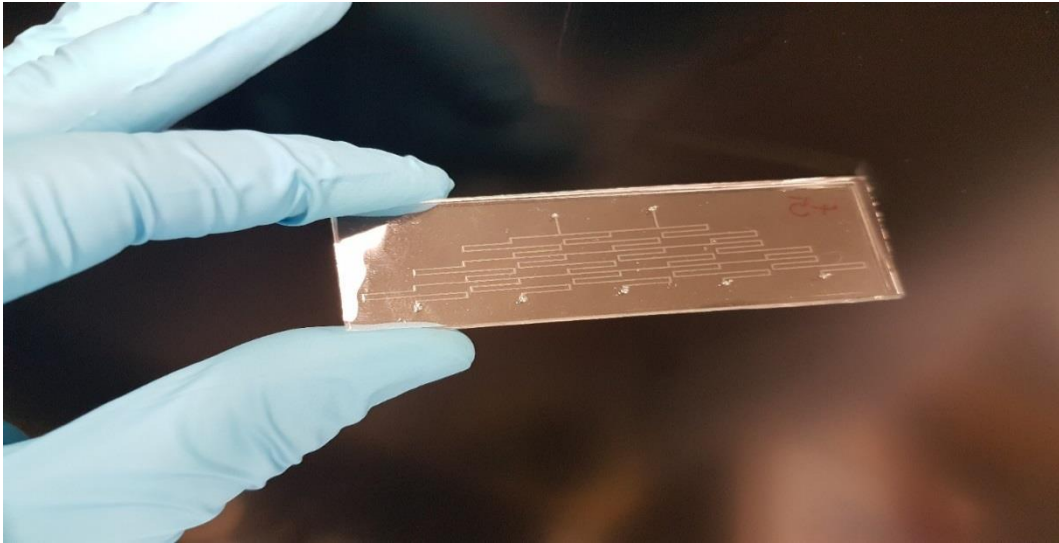


Figure 1: PDMS-based microfluidic gradient generator.

Lab-on-chip (LOC) and micro total analysis systems (μ TAS) as shown in Figure 2 aim for the integration and miniaturization of multiple chemical and biological functions, including sample preparation and analysis [11]. The most frequently used LOC systems have integrated electrochemical or optical biosensors similar to bioreactors enabling non-invasive monitoring and/or analysis of biological samples such as cell cultures or blood.



Figure 2: Schematic images of a lab-on-chip device [11], [12].

A more biotechnological application of LOC systems is the microfluidic chemostat that maintains and analyses microbial populations using complex multi-layered microchannels in combination with a high density of pneumatic microvalves [1], as shown in Figure 3.

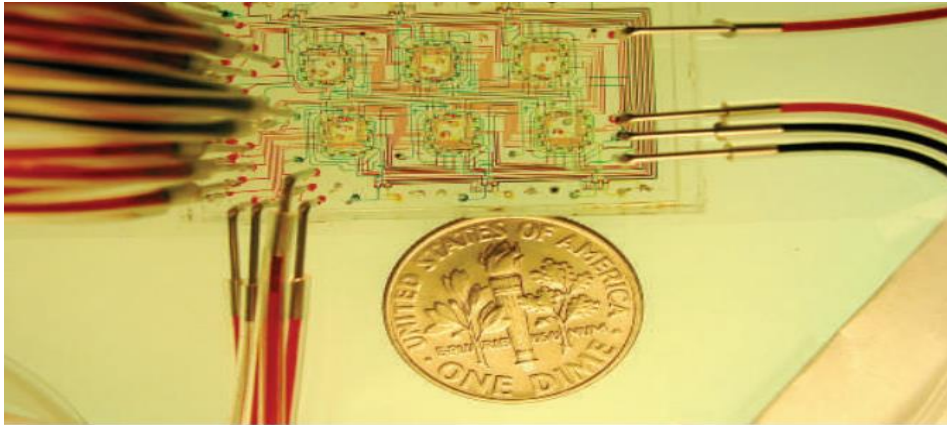


Figure 3: a Microfluidic chemostat study the growth of microbial populations, integrated with pneumatic valves [1].

In contrast to such highly integrated systems, microfluidic immunoassays work on the principle method of detecting pathogenic agents and are heavily used as systems for medical diagnostics. For instance, miniaturized mosaic immunoassays are presented based on lines of antigens on a surface [13], as shown in figure 3, where a sequence of immobilization, blocking and detection steps are performed to result in a high throughput diagnostic system.

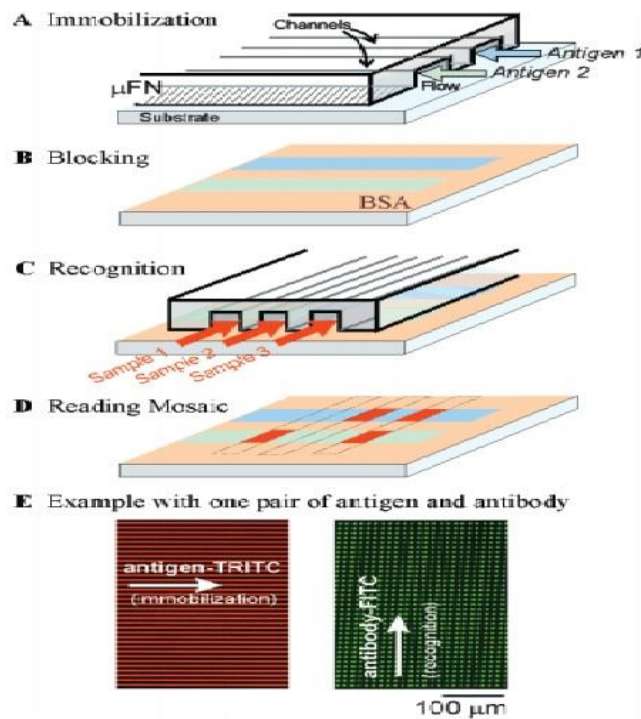


Figure 4: Schematic of Micro mosaic Immunoassay preparation and its multiple stages: a) immobilization, b) blocking, c) recognition, d) reading mosaic [13].

2.2 MICROFLUIDIC GRADIENT GENERATORS

Concentration gradients play a critical role in the human body and control many essential functions like embryogenesis, immune response, development, cancer metastasis [14], inflammation, cell signaling pathways, wound healing, growth of cells [15], drug delivery and chemotaxis [16]. It also play a critical rule in chemical (nucleation and growth of crystals) [17]. By investigating and observation of the interactions between molecular gradients and their cellular reactions, many unknown functions and phenomena in the human body and in biology will be solved [18]. For that purpose, scientist and engineers work together closely to mimic and simulate these concentration gradients in the laboratory [18]. The rise of gradients in biological systems started early with tool like the Boyden chamber [19], Dunn slide chamber [14], pipette injection methods, as well as the integration of porous hydrogels [20]. In later years, for instance agarose-Petri dishes [14] were used, however, the resolution accomplished by was still very macroscopic. In turn, a microfluidic gradient generator can precisely control gradients at the micro and nanoscale. For instance, human cells have a diameter in a range of 10-100 μm , and the intercellular signals transduction length caused by diffusion limit in tissue is roughly around 250 μm [21]. Therefore, the scaling of microsystem should ideally be in the same magnitude. In general, Microfluidic gradient generators have some advantages like: Easy to control and maintained, portable, low consumptions of reagents and low fabrication costs.

2.2.1 Types of microfluidic gradient generator designs

2.2.1.1 Tree-shape microfluidic gradient generator

It is one of the first microfluidic gradient generator designs and widely spread due to the simple design and fabrication processes. But it has also some disadvantages as high shear stress, and possibility of chip leakage and channel obstruction/blocking. Similar to the tree-shape gradient generators, T- and Y-shaped designs have the advantage of start mixing at an early stage and guarantee more efficiency (mixing starts earlier and more mixing time and mixing space) [18]. This method is used to screen compounds on the single cell level [22]. Figure 5 shows an example of Y-shape microfluidic gradient generator.

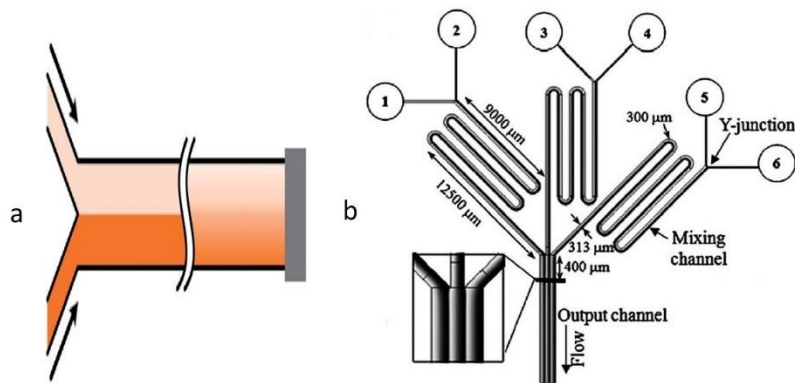


Figure 5: Y-shape microfluidic gradient generator [18].

2.2.1.2 Multi-layer concentration gradient generator based on membrane systems

A chemical gradient is generated in the bottom layer and diffuses through the PDMS layer into the cell culture wells in the top layer [18]. Figure 6 shows an example membrane microfluidic gradient generator. This system uses porous membranes to separate the fluid flowing from the gradient generation chamber, to be sure that only solute molecules will diffuse through.

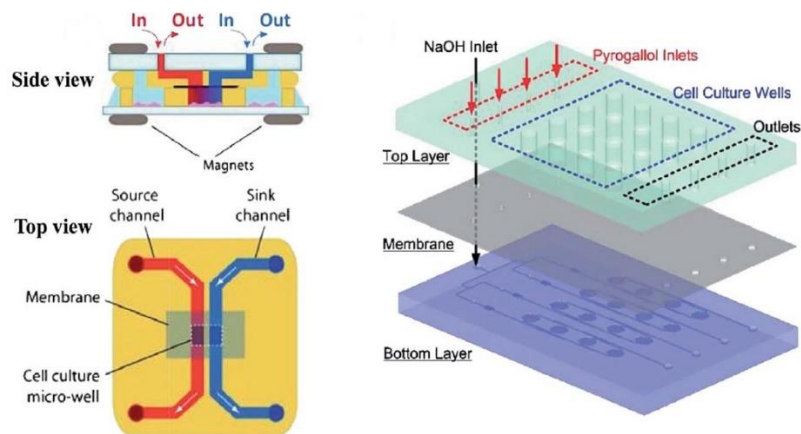


Figure 6: Multi-layer concentration gradient generator of membrane systems [18]

The diffusion between the reagent and the buffer are slowly increasing until it reaches stable gradients. This system has simple a structure and has no shearing, but the speed of generation is low [18].

2.2.1.3 Pressure balance microfluidic gradient generators

For pressure balance gradient generators in contrast to membrane system, where a membrane stops the fluid flowing, high control of flow rates and pressures in inlet and outlet at both convection units must be guaranteed until the pressure is balanced among all the units. Consequently, the mixing by convection does not happen but pure diffusion happens in the channels [23], [24]. Another advantage of this gradient generator is that stable gradients still can be achieved even at low flow rates, as long as these flow rates are above certain critical values [25]. Figure 7 shows an example of a pressure balance microfluidic gradient generator.

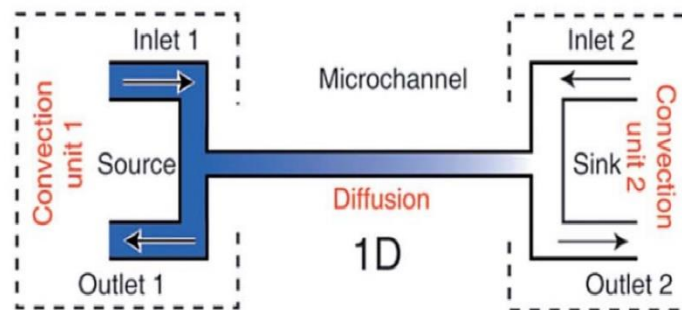


Figure 7: Single layer microfluidic pressure balance gradient generator [18]

2.2.1.4 Droplet generation microfluidic gradient generator

This type of gradient generators creates monodisperse droplets with diverse concentrations. Here, the concentration of the spreaded phase has to be adjusted over the time as generated droplets have the identical chemical concentration with spreaded phase. To retain the droplet size, the flow rates for the continuous phase and spreaded phase have to be fixed [23], [24]. Additionally, multiple inlets are usually used to obtain different fluid concentrations [28]. Figure 8 shows an example of droplet microfluidic gradient generator.

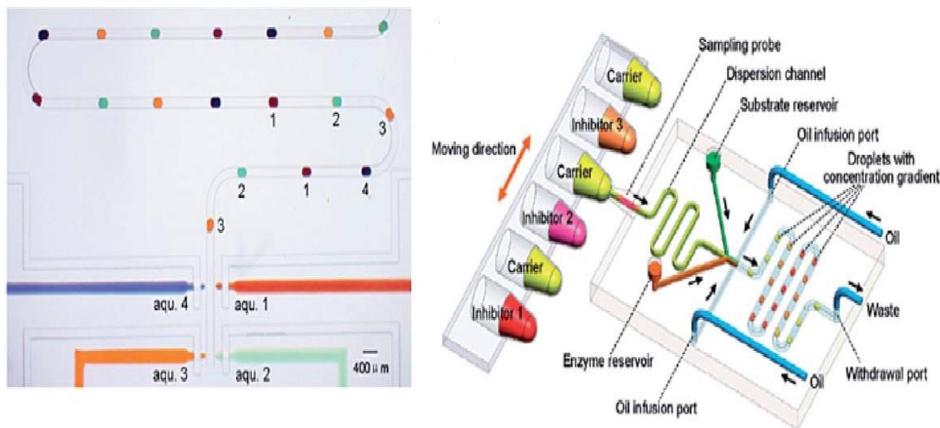


Figure 8: Droplet generation microfluidic system to gain molecular gradients [18].

2.3 FLUID MECHANICS IN MICROFLUIDIC CHANNELS

The behavior of a fluid, which may contain particle suspensions, flowing in micro-dimensional channels is governed by both viscous and surface tension forces as well as high shear rates and geometric effects. The following section discusses some of the key transport phenomena affecting fluid mechanics in micro-engineered devices.

2.3.1 Transport Phenomena

Transport phenomena study the swap of mass, heat and momentum between two interacted systems. It centers on the state of sharing features or attributes between the mass, heat and transport, which have the same mathematical framework [29]. Transport phenomena is a permanent action (unable to be undone) originated by random movement of molecules, that occur especially in fluids. It depends on two fundamental laws: conservation law (the sum the studied quantities should be conserved) and constitutive equations (how the material react to external stimuli).

2.3.2 Navier-Stokes equation

A notable example of transport phenomena is the Navier-stokes equation, which describes the influence of applied forces on the fluid. Therefore, the Navier-stokes equation describes the dynamics of fluids in microfluidic gradient generators. This equation is used for incompressible Newtonian fluids, whereas the fluid is incompressible as the volume changes are minor and very small when the pressure changes [30]. Water and fluorescein dye are considered Newtonian fluids [31]. It describes the rate of change in a fluid momentum with convective, viscous and pressure forces as shown in equation

1:

$$\rho \frac{d\vec{u}}{dt} = -\rho\vec{u} \cdot \nabla\vec{u} + \mu\nabla^2\vec{u} - \nabla P + \vec{F} \quad \text{Equation 1}$$

Rate of change of momentum
 = convection force + viscous force + pressure force

ρ : density of the flow (kg/m³), U : the velocity vector of the fluid(m/s), it gives the velocity in a certain point and time $\vec{u} = \vec{u}(\vec{r}, t)$,

μ : dynamic viscosity (Pa*s),

∇P : the pressure gradient (Pa),

F : the external force applied on fluid. The temperature is presumed as constant (room temperature ~ 20°C), so the viscosity is still constant. In laminar flow and constant flow, the equation becomes:

$$\nabla P = \mu\nabla^2\vec{u} \quad \text{Equation 2}$$

2.3.3 Reynolds Number

It is a dimensionless number in fluid mechanics that determines and predicts whether the flow is laminar or turbulent, named after Osborne Reynolds. Can be defined as the ratio between inertial forces and viscous forces, as it shown in equation (11)

$$Re = \frac{\text{inertial forces}}{\text{viscous forces}} \quad \text{Equation 3}$$

Where:

Inertial force (ρV^2) involves force due to the momentum of fluid mass (try to push the fluid movement forward). Viscous force ($\frac{\mu V}{L}$) is the force that slows down the fluid (friction force). An example to clarify it is the comparing between pouring a cup of honey and pouring a cup of water. The honey has a higher viscosity because it is more resistance to flow than the water.

$Re < 1$ Viscous effect dominant over Inertial effects (microfluidic).

$Re > 1$ Inertial effect dominant over Viscous effects.

Reynolds number can be described also as shown in equation 4:

$$Re = \frac{\rho v L}{\mu} \quad \text{Equation 4}$$

Where:

ρ : density of the flow (kg/m^3),

V: velocity of the flow (m/sec),

L: characteristic length of the fluid channel (m),

μ : dynamic viscosity ($\text{Pa}\cdot\text{s}$).

according to Reynolds number, there are three different flow regimes:

- Laminar flow: $\text{Re} < 2300$. It has many characteristics and advantages as: low velocity, the particles move along well-defined paths or streamlines, all streamlines are straight and parallel to each other and to the surface at different speeds with no mixing, most of the energy losses due to viscous effects, viscous forces are dominant and inertial forces are negligible, easy to calculate and simulate and analyze.
- Turbulence flow: $\text{Re} > 4000$. unsteady flow, fluid particles move along irregular paths, velocity is high, inertial forces are dominant and viscous forces are negligible.
- Transition flow: $2300 < \text{Re} < 4000$. The flow status is changing between the laminar and turbulence flow.

In microchannels, the flow rates are low and the dimensions scales are small and the inertial effects such as gravity-based separation and secondary flow and turbulence are negligible [32], [33]. Applying the Reynolds number equation to any microfluidic channel, the result is simple: flow is always laminar in microsystems.

$$Re = \frac{\text{inertia forces}}{\text{viscous forces}} = \frac{\rho \cdot V \cdot D}{\mu}$$

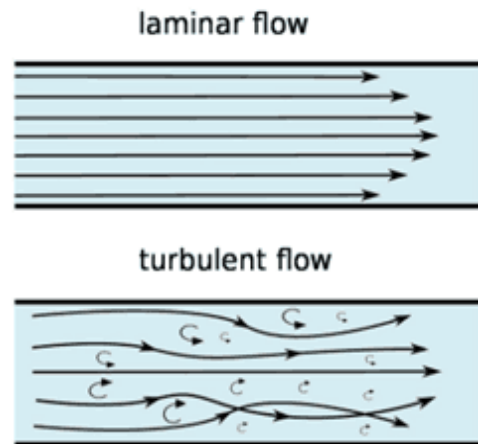
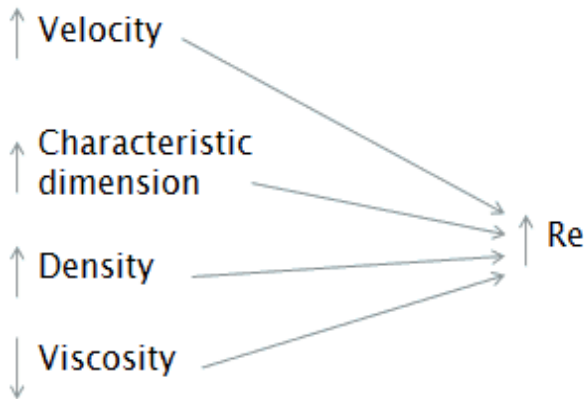


Figure 9: Laminar flow versus turbulent flow and the Reynolds number [34].

The velocity of the flow V can be calculated by applying the volumetric flow rate equation

$$Q = V \cdot A \quad \text{Equation 5}$$

Where:

Q : volumetric flow rate (m^3/s),

V : velocity (m/s),

A : cross-sectional area of the fluid perpendicular to flow (m^2). In this thesis, the channels are rectangular ducts, so Hydraulic Diameter equation is applied:

$$D_h = \frac{4 \cdot A}{P} \quad \text{Equation 6}$$

Where:

D_h : hydraulic diameter (m),

A : cross-section area (m^2),

P : the wetted perimeter of the channel, in contact with the fluid (m).

For rectangular channels D become:

$$D_h = \frac{4ab}{2(a+b)} = \frac{2ab}{a+b} \quad \text{Equation 7}$$

Where:

- a: width of the rectangular duct (m),
- b: height of the rectangular duct (m)

2.3.4 Hagen-Poiseuille's law

The volumetric flow rate, which is the volume of fluid flowing per unit time (m³/s) can be described by Hagen-Poiseuille's law as shown in equation 7:

$$Q = \frac{\pi R^4}{8\mu} \left(-\frac{dp}{dx} \right) \quad \text{Equation 8}$$

This equation is applied for straightforward and infinite long channels. But can be also applied on the finite channel with length L, if we assume $L/R \gg 1$ and $L/R \gg Re$ and the pressure gradient is regular and steady, then $-\frac{dp}{dx}$ can be convergent to $\frac{\Delta P}{L}$ and the equation becomes:

$$Q = \frac{\pi R^4 \Delta P}{8\mu L} \quad \text{Equation 9}$$

The Hagen–Poiseuille equation is usually applied to simplify fluid flow in microfluidic networks into equivalent hydraulic circuits, analogous to electric circuits (see Table 1) [14].

2.3.5 Hydraulic Resistance

Hydraulic circuit analysis is useful for determining the concentration value of individual output streams in gradient generators such as the “Christmas tree” design. The Hagen-Poiseuille equation can be simplified to:

$$Q = \frac{\Delta P}{R_H} \quad \text{Equation 10}$$

$$\Delta P = Q \cdot R_H$$

$$R_H = \frac{8\mu L}{\pi R^4} = \frac{8\mu L}{\pi r_H^4} \quad \text{Equation 11}$$

Where:

R_H : hydraulic resistance (Pa*s³*m⁻¹)

For non-circular channels $D_H = 2r_H$, $D_H = 4A/P$, $r_H = 2A/P$

A: cross section area (m²), P: wetted perimeter, in contact with the fluid, (m).

For rectangular microchannel, hydraulic resistance become:

$$R_H = \frac{12\mu L}{wh^3 \left(1 - \frac{h}{w} \left(\frac{192}{\pi^5} \sum_{n=1,2,3}^{\infty} \frac{1}{n^5} \tanh \left(\frac{n\pi w}{2h} \right) \right) \right)} \quad \text{Equation 12}$$

When $h/w \ll 1$, R_H becomes:

$$R_H = \frac{12\mu L}{wh^3} \quad \text{Equation 13}$$

$$R_H = C_{geometry} \mu \frac{L}{A^2} \quad \text{Equation 14}$$

$C_{geometry}$: geometric coefficient, for rectangular channels [35] :

$$C_{geometry} = \frac{12*(w/h)}{1 - \frac{h}{w} \left(\frac{192}{\pi^5} \sum_{n=1,2,3}^{\infty} \frac{1}{n^5} \tanh \left(\frac{n\pi w}{2h} \right) \right)} \quad \text{Equation 15}$$

From hydraulic resistance equation, the hydraulic resistance is proportional to the microchannel length ($R_H \sim L$). and the hydraulic resistance is constant for normal laminar flow and normal geometric state. To simplify the study, the tree shape microfluidic gradient generator can be compared to an equivalent electric circuit [14]. The similarity between the hydraulic circuit and the electric circuit are shown in Table 1:

Table 1: Similarity between electric and hydraulic circuit.

Electric circuit	Hydraulic circuit
R electrical resistance	R_H hydraulic resistance
I electrical current	Q flow rate
ΔV electrical voltage	ΔP pressure drop
$\Delta V = RI$ Ohm law	$\Delta P = R_H Q$ Hagen poiseuille equation
Electrical resistance series combination: $R_{eq} = R_1 + R_2 + R_3 + \dots + R_n$	Hydraulic resistance series combination: $R_{Heq} = R_{H1} + R_{H2} + R_{H3} + \dots + R_{Hn}$
Electrical resistance parallel combination: $\frac{1}{R_{eq}} = \frac{1}{R_1} + \frac{1}{R_2} + \frac{1}{R_3} + \dots + \frac{1}{R_n}$	Hydraulic resistance parallel combination: $\frac{1}{R_{Heq}} = \frac{1}{R_{H1}} + \frac{1}{R_{H2}} + \frac{1}{R_{H3}} + \dots + \frac{1}{R_{Hn}}$
Kirchhoff current law:	Navier-Strock equation:

At node n: $\sum_{i=1}^n I_i = 0$	At node n: $\sum_{i=1}^n Q_i = 0$
n: number of branches with currents going into or away from this node.	n: number of channels with flow going into or away from this node.
Source: Motor	Source: Syringe pump

Only the resistance of the vertical channels needs to be considered in hydraulic circuit.



Figure 10: Similarity between electric circuit and hydraulic circuit [14].

For the electric circuit:

At node 1:

$$I_3 = \left(\frac{R_2}{R_1 + R_2} \right) I_1$$

$$I_4 = \left(\frac{R_1}{R_1 + R_2} \right) I_2$$

At node 3:

$$I_5 = \left(\frac{R_3}{R_2 + R_3} \right) I_2$$

$$I_6 = \left(\frac{R_2}{R_2 + R_3} \right) I_2$$

At node 2:

$$I_4 + I_5 =$$

$$I_4 + I_5 = \left(\frac{R_1}{R_1 + R_2} \right) I_1 + \left(\frac{R_3}{R_2 + R_3} \right) I_2$$

For the hydraulic circuit:

At node 1:

$$Q_3 = \left(\frac{R_{f2}}{R_{f1} + R_{f2}} \right) Q_1$$

$$Q_4 = \left(\frac{R_{f1}}{R_{f1} + R_{f2}} \right) Q_1$$

At node 3:

$$Q_5 = \left(\frac{R_{f3}}{R_{f2} + R_{f3}} \right) Q_2$$

$$Q_6 = \left(\frac{R_{f2}}{R_{f2} + R_{f3}} \right) Q_2$$

At node 2:

$$Q_4 + Q_5 = \left(\frac{R_{f1}}{R_{f1} + R_{f2}} \right) Q_1 + \left(\frac{R_{f3}}{R_{f2} + R_{f3}} \right) Q_2$$

The concentration of flow in mixer R_{f2} :

$$C_{R_{f2}} = \frac{Q_4 \cdot C_0 + Q_5 \cdot C_1}{(Q_4 + Q_5)} \quad \text{Equation 16}$$

In general, the concentration of any mixer module:

$$C_{\text{mixer module}} = \frac{\sum_{i=1}^2 Q_i \cdot C_i}{\sum_{i=1}^2 Q_i} \quad \text{Equation 17}$$

Where i is the streams come at certain node (left & right).

2.3.6 Mixing phenomena

Microfluidic gradient generators can be classified into two categories according to their gradient generating principles: laminar flow diffusion-based gradient generator and convection mixing-based gradient generators.

2.3.6.1 Diffusion

Diffusion is a mass transport phenomenon which results in the distribution of a chemical species to turn into more homogenous and steady in space as time evolving [36]. (does not happen due to the activity of force but as a result of random movement of molecules). It is also the transport of the molecules from a higher concentration region to lower concentration region smoothly and deterministically by random motion. The origin of diffusion comes from the thermal motion of molecules. The molecules are always in motion when the temperature is higher than zero. They hit each other frequently every few nanoseconds so the orientation of their movement turns into randomize. So, the molecules move and constantly change their orientation, so the diffusion happens as a reason of the statistic of this movement [37]. The time needed to mix related to the diffusivity (D) and length scale to homogenize the concentration:

$$X = \sqrt{2Dt} \quad \text{Equation 18}$$

Where:

X: diffusion length (m), D: diffusion coefficient (m²/s), t: time (s).

The best way to describe the diffusion theory comes by Adolf Fick in 19th century with two laws (Fick's first diffusion law and Fick's second diffusion law):

- Fick's first diffusion law: (for steady state system)

Flow which caused by diffusion is proportional to the concentration gradient.

$$J = -D \frac{dc}{dx} \quad \text{Equation 19}$$

Where:

J: Flux of particles (mol.m⁻²*s⁻¹),

D: diffusion coefficient or diffusivity (m²*s⁻¹),

dc/dx: concentration gradient.

Minus sign (-) means that the flux direction from high concentration to the low concentration, in other words, reverse to the concentration gradient.

Fick's first diffusion law characterized by the diffusion coefficient or diffusivity (D), which measure the average of the diffusion operation. Diffusion coefficient (D) depends on: diffusion mechanism, diffusion temperature, molecule structure, molecule size, molecule imperfection, solute concentration. The radius of molecule effects the diffusivity, small molecules have higher diffusivity:

$$D = \frac{kT}{6\pi\mu r} \quad \text{Equation 20}$$

D: diffusion coefficient,

k: Boltzman constant,

T: absolute temperature, μ : solvent viscosity,

r: radius of diffusing molecules.

Temperature affects the diffusivity, higher temperature means higher diffusivity and higher diffusion rate:

$$D = D_0 e^{-\frac{E_A}{RT}} \quad \text{Equation 21}$$

D: diffusion coefficient (m^2/s),

D_0 : proportionality constant independent of absolute temperature (m^2/s), E_A : activation energy for diffusing species (J/mol),

R: constant ($R = 8.314 \text{ J/mol. k}$),

T: absolute temperature.

- Fick's second diffusion law: (non-steady state diffusion)

The concentration changing rate at a certain point is proportional to the second derivation of concentration. It is a linear equation anticipate the change of diffusion with time, and the diffusion happened independently for each chemical species. All these properties

make the mass transport system that described by Fick's second diffusion law is easy to simulate [38].

$$\frac{dCx}{dt} = D\left(\frac{\partial^2 C}{\partial x^2} + \frac{\partial^2 C}{\partial y^2} + \frac{\partial^2 C}{\partial z^2}\right) \quad \text{Equation 22}$$

2.3.6.2 Convection

Convection is a mass transport phenomenon due to bulk motion of fluids. Different from diffusion, convection occurs due to intermediate velocities of all molecules, while diffusion happens due to random velocities of individual molecules [39]. It is important to mention that convection is not involved in mixing within microchannels, but diffusion is the only mass transport phenomenon involved with microfluidic devices [40], [14], [39]. Additionally, the Péclet number is a dimensionless number, defined to be the rate of convection transport on diffusion transport as:

$$Pe = \frac{N_{convection}}{N_{diffusion}} = \frac{UC}{D_L} = \frac{UL}{D} \quad \text{Equation 23}$$

Where:

U: flow velocity (m/s), L: characteristic length (m),

D: diffusivity (m²/s).

When $Pe \gg 1$, convection is dominating the mass transport in the system.

$Pe \ll 1$, diffusion is dominating the mass transport in the system.

In microfluidic $Pe \ll 1$, meaning that diffusion dominates the mass transport in microfluidic and this is in accordance to earlier mentioned theories.

3 GOALS OF THE THESIS

In this thesis, the design, CFD modeling and characterization of a microfluidic concentration gradient generator will be discussed that requires flowing fluid streams to develop a stable chemical gradient. An optimal microfluidic gradient generator design for rapid prototyping processes was drafted, designed and fabricated by photolithography, UV injection molding and soft lithography. As microfluidic devices become increasingly complex, their design and optimization based on experiments become difficult. In this respect, numerical simulations based on Computational Fluid Dynamics (CFD) technologies help to gain a better understanding of the physical phenomena taking place and hence to offer a powerful design tool in optimizing the performance of microfluidic devices. The microfabricated chips were characterized regarding flow profile, molecular concentration profiles and flowthrough volume by gravimetric and spectroscopic evaluation in comparison to CFD simulation. The overall aim is to predict the flow patterns, pressures and velocities throughout the microfluidic r design and, in particular, to investigate the effect of three channel heights and inlet-outlet conditions on the separation efficiency. Specific fluid dynamics and physical considerations are presented in the first part of the thesis. In the second part, the simulation and experimental results are presented for nine different flow rates.

- Laminator (Heat Seal H520 high speed personal Laminator, Acco Brands)
- Exposure Masking System (UV-Kub 2, Kloe)
- Heating Plate (Torrey Pines-scientific)
- Plasma cleaner (PDC-002-CE, Harrick plasma)
- Oven (Binder)
- Air gun (BANCO)
- Isopropanol (98%)
- Deionized H₂O
- PDMS
- Petri dish

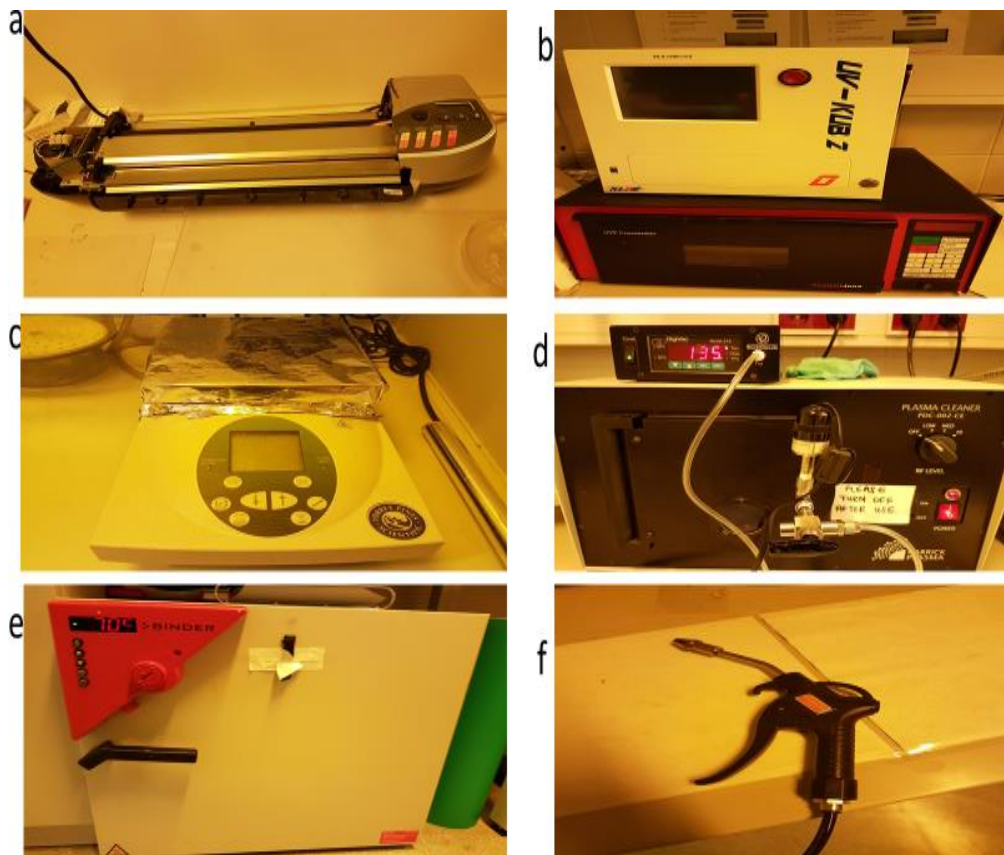


Figure 12: Master Mold fabrication tools: a) Laminator. b) Exposure masking system. c) Heating plate. d) Plasma cleaner. e) Oven. f) Nitrogen guns.

4.2.2 Fabrication procedure

For 45 μm and 90 μm high devices, the epoxy-based dry film resist (DFR) TMMF S2030/45 (Tokyo Ohka Kogyo Co. Ltd) was used for microfabrication of master molds in the range between 30 μm and 90 μm channel height for PDMS soft lithography. Prior to lamination silicon wafers were sonicated in 2% Hellmanex III solution (Hellma Analytics), deionized

H₂O and isopropanol for 10 minutes at 30 °C. The DFR was laminated under heat to the wafer using a HeatSeal H425 A3 office laminator (GBC) to achieve 45 µm and 90 µm height structures. Following lamination, a polymer film mask (Photo Data Ltd, UK) was applied and the wafer was exposed to UV light using a mask aligner (EVG 620). For TMMF crosslinking, a postexposure bake (PEB) was performed at 90°C for 5 minutes. The resist was then developed in EBR solvent (PGMEA/1-methoxy-2-propyl-acetate, MicroChemicals) under magnetic stirring until non-crosslinked TMMF was completely removed from the wafer surface (typically after around 90 seconds) followed by isopropanol and dH₂O rinsing. Next, the developed and N₂ blow-dried photoresist structure was hard-baked in an oven at 200 °C for 1 hour. All structured wafers were plasma-treated and fluorinated using a Teflon-like silane (trichloro(1H,1H₂H,2H-perfluorooctyl)silane) (Sigma-Aldrich) prior replica molding of PDMS and OSTEMER devices.

4.3 FABRICATION OF THE GRADIENT GENERATOR USING OSTEMER

4.3.1 Fabrication tools

- OSTEMER two-component kit(Mercene Lab)
- Analytical Balance (VWR LA 254i, max 250g)
- Vortex (VELP SCIENTIFICA)
- Degasser (VWR)
- Isopropanol (98%)
- Convection oven (Binder)
- Glass slides (VWR, cut edges)

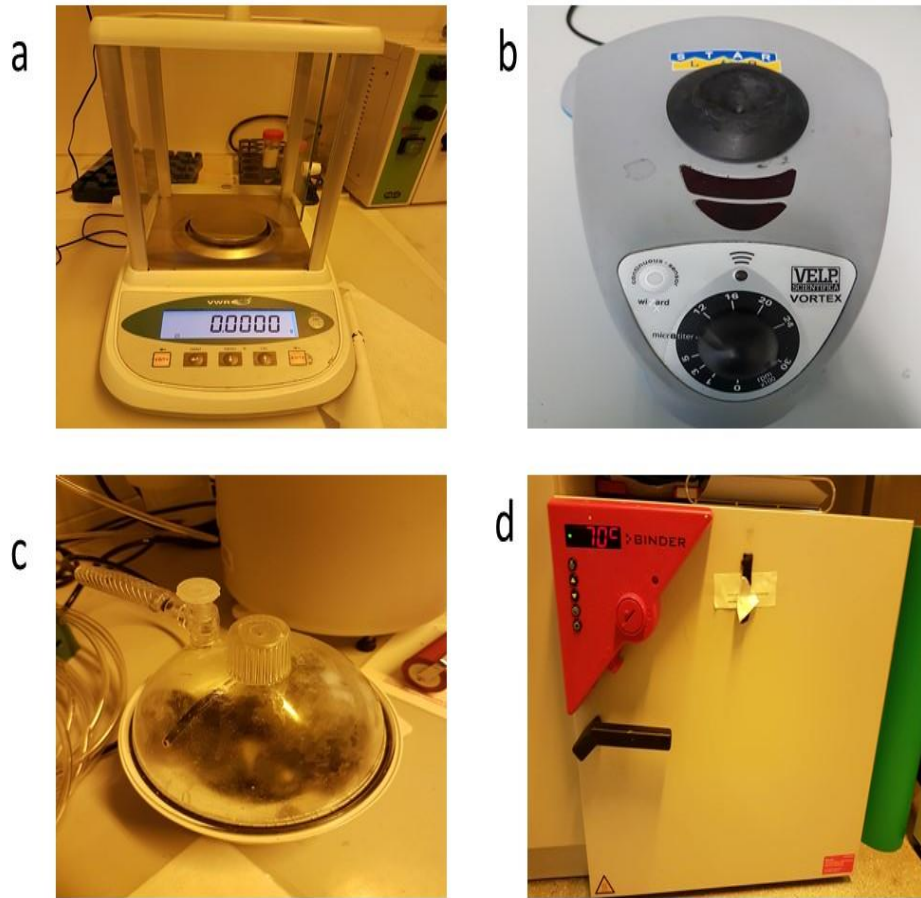


Figure 13: Fabrication of the gradient generator using OSTEMER tools. a) Analytical balance. b) Vortex. c) Degasser. d) Oven.

4.3.2 Fabrication procedure

OSTEMER is a paired polymer (UV + heat) with high transparency and capacity to ligament and merge to several materials. It is colorless and has viscosity equal $4000 \text{ m} \cdot \text{pas}$ [41]. For fabrication of the microfluidic gradient generator, OSTEMER (322-40 crystal clear, Mercene Labs AB, Sweden) was used, as shown in Figure 14:



Figure 14: OSTEMER two components

The two components of OSTEMER (A, B) were mixed, the mixing ratio is (A: B is 1.09 to 1) [41], and the components were weighted inside glass container using the analytical balance (A=4 g, B=4.36 g), then mix them using the vortex for about 5 minutes for homogenization of the viscous components and rest them for about 30 minutes inside the degasser machine to get rid of the gas bubbles[42]. After that, the mixing was cured by 365 nm wavelength Hg-tubes in crosslinker provided with energy irradiation sensor (Bio-link BLX Crosslinker, Vilber Lourmat). Replica molding of OSTEMER microfluidics involved casting of the polymer mix on fluorinated PDMS master molds. A 250 μm PDMS film (MVQ silicones) was used to adjust the total height of the microfluidic layers and create a flat surface. Following UV exposure at a dose of 700 mJ/cm^2 , the OSTEMER device was delaminated, developed with isopropanol and dried. Fluid interface holes were drilled using a conventional benchtop drill followed by extensive rinsing with isopropanol. For final chip assembly, the OSTEMER replica as well as an unstructured OSTEMER layer with 250 μm thickness were aligned, fixed in place and baked at 110 $^{\circ}\text{C}$ overnight to ensure that all layers were bonded properly.

4.4 FABRICATION OF MICROFLUIDIC GRADIENT GENERATOR BY USING PDMS

4.4.1 Fabrication tools

- PDMS (dimethylpolysiloxane or dimethicone): Is a mineral-organic polymer which belongs to the silicone group and has following formula: $(\text{C}_2\text{H}_6\text{OSi})_n$, n, whereas the number of monomer repetitions [43], as shown in Figure 18:

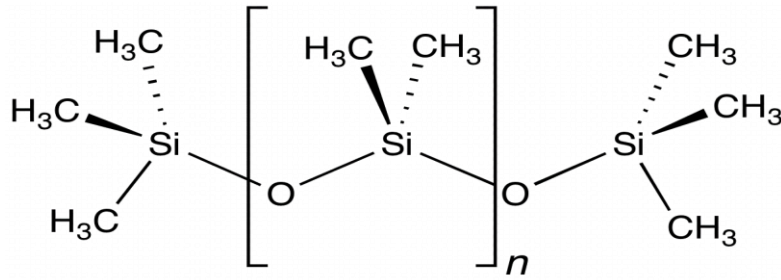


Figure 15: PDMS structure [44].

It has been vastly used in microfluidic fabrications due to its properties, such as low costs compared to other materials, optical transparency which allows observing the flow inside the microchannels even by naked eyes and easy fabrication [45]. This biocompatible material (with some limitations) has a low autofluorescence [46], it is gas permeable and it can be bonded to glass or other PDMS layers, it has hydrophobic surface [47]. All these advantages make PDMS the best choice for the gradient generator fabrication. The liquid PDMS base used in this fabrication was Sylgard 184 Silicone Elastomer base and its curing agent, as shown in Figure 17:

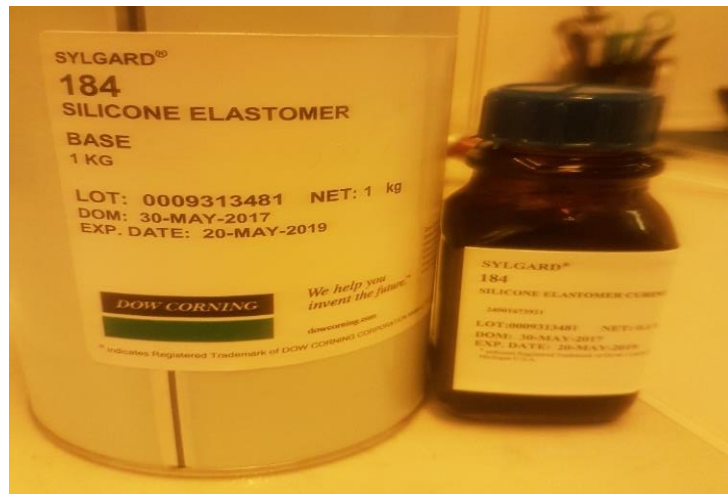


Figure 16: Silicone elastomer and its curing agent.

- Convection oven (Binder)
- Plasma cleaner (PDC-002-CE, Harrick plasma)
- Degasser (VWR)
- Isopropanol (98%)
- Deionized H₂O
- Glass slides (VWR, cut edges)

4.4.2 Fabrication procedure

The two components of PDMS (Sylgard 184 and its curing agent) were mixed in ratio 10:1, (base=30 ml, curing agent=3 ml), mixed and poured on the master mold to form a 3-4 mm thick PDMS layer and baked overnight at 70°C. Prior plasma bonding on cleaned glass object slides (high power, 2 minutes; Harrick Plasma), holes for tubing interconnection (inlets and outlets) were punched using 1 mm biopsy punches (Kai medical). After plasma-treatment of both layers, PDMS and glass were brought into contact and baked for 1 hour at 80°C. Alternatively, PDMS devices were sealed off with ARseal silicon pressure sensitive adhesive (Adhesive Research) laminated on clean glass slides and gently pressed together to create a stable bond.

4.5 EVALUATION OF THE MICROFLUIDIC GRADIENT GENERATOR

4.5.1 Experimental set-up tools

- Microfluidic gradient generator chip
- Syringe pump (KD Scientific LEGATO 270)
- Microscope (Hund-Wetzlar)
- Two syringes (Terumo syringe 10ml luer lock)
- Tygon Tubes (SAINT-GOBAIN tygon 0.51)
- Eppendorf tubes (Greiner bio-one, 1.5 ml, PP)

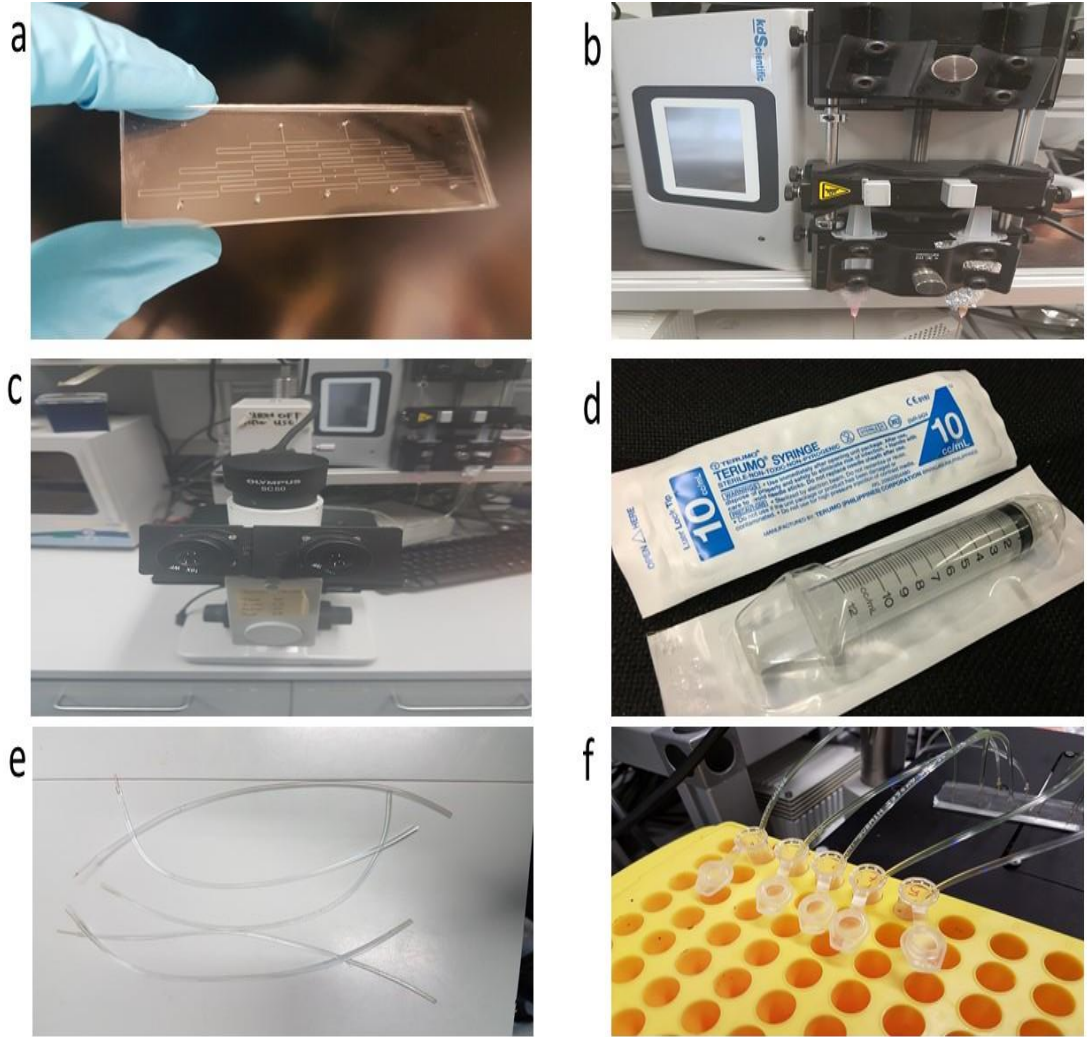


Figure 17: Experimental setup tools: a) microfluidic gradient generator chip. b) syringe pump. c) microscopy. d) two syringes. e) Tygon tubes. f) Eppendorf tubes

- Deionized H₂O
- Fluorescein: It is an organic compound and dye and used as a fluorescent tracer. Its empirical formula is C₂₀H₁₀Na₂O₅ as shown in figure 19. Its excitation wavelength is 460 nm and the emission wavelength is 515 nm [48]. Its appearance color in powder form is orange to brown, and insolubility form is dark yellow to orange-green [49]. In this experiment fluorescein sodium salt Sigma Aldrich F6377-100g was used.

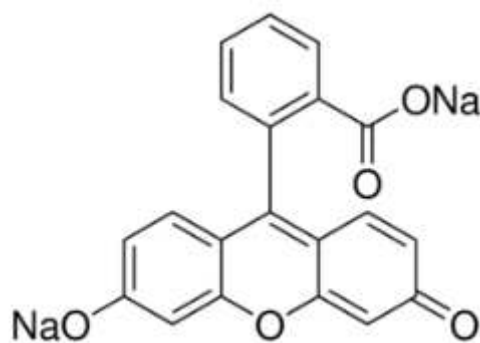


Figure 18: Fluorescein structure

4.5.2 Set-up procedure

The two inlets of the microfluidic gradient generator chip were connected by two tygon tubes to two syringes which they were attached to the syringe, while the five outlets were connected by five tubes to the Eppendorf tubes, each one of these tubes was labeled with its corresponding outlet. One of the syringes was filled with fluorescein and the other syringe is filled with deionized water. A schematic set-up is shown in Figure 20:

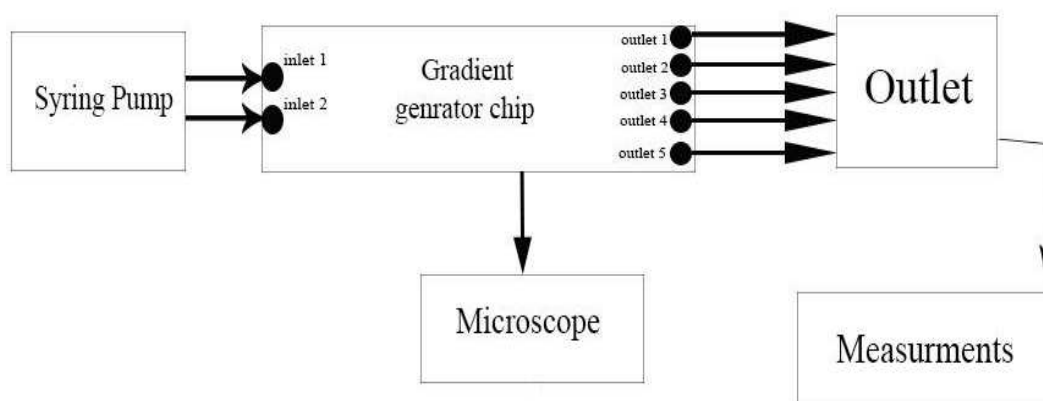


Figure 19: Boxing diagram of the set-up.

After completing the set-up, the measurement started by checking the parameters on the pump monitor. The volume of each syringe was set at 500 μL , that means the total volume infused through the microfluidic gradient generator by both syringes is 1000 μL . Then, the flow rate was defined. Beginning with the highest flow rate 100 $\mu\text{L}/\text{min}$, then 80 $\mu\text{L}/\text{min}$, 60 $\mu\text{L}/\text{min}$, 40 $\mu\text{L}/\text{min}$, 20 $\mu\text{L}/\text{min}$, 10 $\mu\text{L}/\text{min}$, 5 $\mu\text{L}/\text{min}$, 1 $\mu\text{L}/\text{min}$, 0.5 $\mu\text{L}/\text{min}$. The measurement at highest flow rate (100 $\mu\text{L}/\text{min}$) takes about 6 minutes, this time will increase with the decreasing of the flow rate. For example, 0.5 $\mu\text{L}/\text{min}$ flow rate will take about 17 hours to complete.

Note: The fluorescein syringe should be covered with aluminum foil because it is photo active. And also, when filling the syringes with fluorescein and water, the air bubbles must be avoided (because they will affect the laminar flow). Figure 20 shows the experimental set-up as it seen in the Lab:



Figure 20: Experimental set-up.

4.5.3 Gravimetric evaluation of microfluidic gradient generator

4.5.3.1 Measurement tools

- Analytical Balance (VWR LA 254i, max 250g)
- Pipette (VWR 100+1000 μ l)
- Pipette tips
- Eppendorf tubes (Greiner bio-one, 1.5 ml, PP)

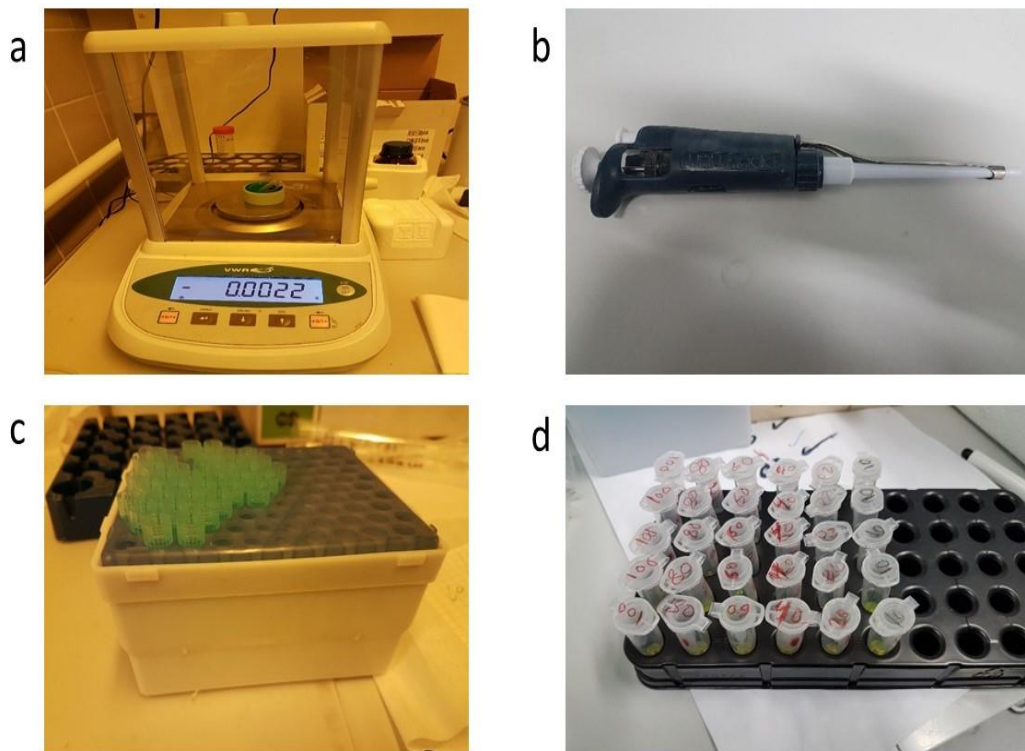


Figure 21: Gravimetric measurement tools: a) Analytical Balance, b) Pipette, c) Pipette tips, d) Eppendorf tubes

4.5.3.2 Measurement procedure

Prior analysis the empty Eppendorf tubes were measured, the analytical balance was reset (make the weight zero), then the empty tube inside the analytical balance was filled with the sample volume that had been aspirated earlier (**note:** the refilling should be done carefully, so the pipette tips should not touch the Eppendorf tube during the liquid filling so the Eppendorf tube does not change its position). At this point the weight is measured, and the pure weight in every Eppendorf tube (outlet) was obtained. This procedure is repeated for every Eppendorf tube (5 Eppendorf tubes for the 9 different flow rates, that means 45 Eppendorf tubes for every chip).

4.5.4 Spectroscopic evaluation of the microfluidic gradient generator

4.5.4.1 Measurement tools

- Multimode Plate Reader (Perkinelmer, EnSpire 2300, Serial Nr.: 23001541)
- Pipette (VWR P200)
- Pipette tips
- Microplate (Greiner bio-one, 96 well, PS, F-bottom)
- Eppendorf tubes (Greiner bio-one, 1.5 ml, PP)

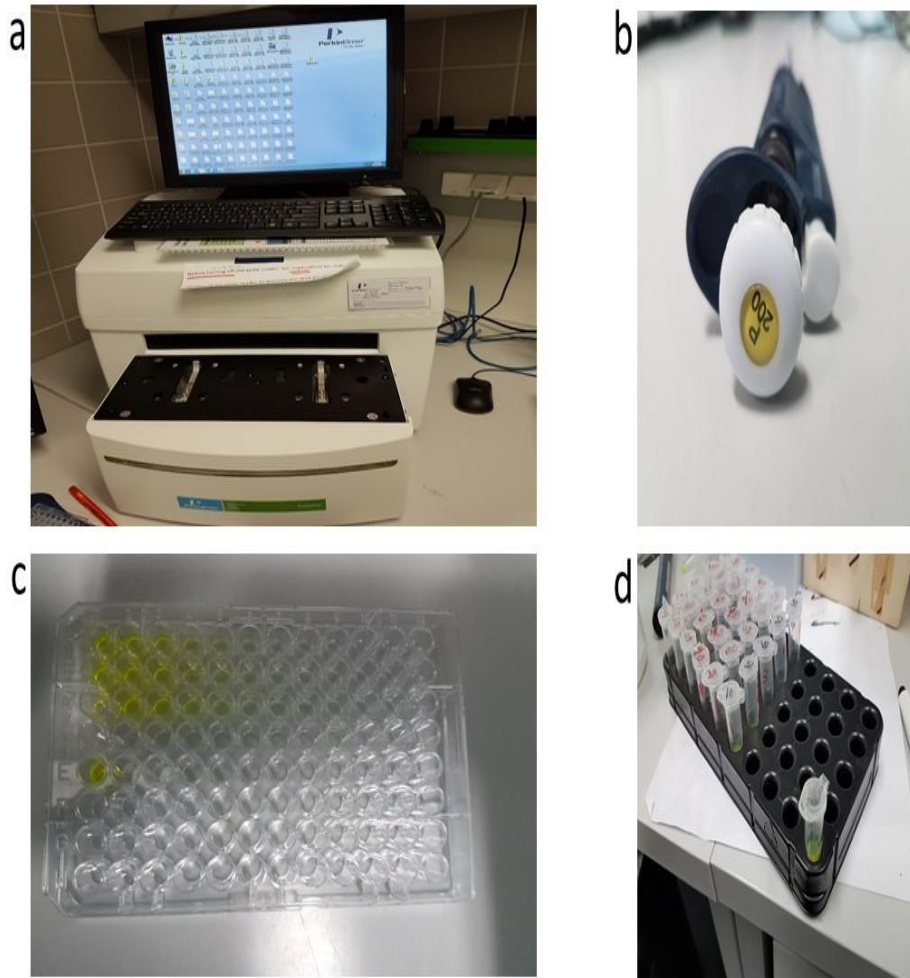


Figure 22: Spectroscopic measurement tools: a) multimode plate reader, b) pipette, c) microplate, d) Eppendorf tubes

4.5.4.2 Measurement procedure

First, the calibration curve was defined, by measuring the fluorescence intensity of 12 different fluorescein concentrations beginning with 100 $\mu\text{g/ml}$, dilute it by 1:2 until reaching 0 $\mu\text{g/ml}$ (pure water). Following concentrations were analyzed in triplicates: 100 $\mu\text{g/mL}$, 50 $\mu\text{g/mL}$, 25 $\mu\text{g/mL}$, 10 $\mu\text{g/ml}$, 5 $\mu\text{g/mL}$, 2.5 $\mu\text{g/mL}$, 1 $\mu\text{g/mL}$, 0.5 $\mu\text{g/mL}$, 0.25 $\mu\text{g/mL}$, 0 $\mu\text{g/mL}$, as shown in figure (9, d). Then, samples were measured by the Multimode Plate Reader to start calibration, considering to the following parameters:

Absorption wavelength = 490 (nm), number of flashes = 10

Excitation wavelength = 460 (nm), Emission wavelength = 515 (nm)

Number of flashes = 20

These results of fluorescein intensity are obtained, as shown in Table 2:

Table 2: Fluorescein intensities results

Fluorescence Intensity (a.u)	Fluorescein concentrations (µg/ml)									
	100	50	25	10	5	2.5	1	0.5	0.25	0
A	175416	167066	1E+05	118254	96351	68997	43527	27594	16244	0
B	180101	166676	1E+05	118540	93503	68105	43867	27473	16142	0
C	179590	167298	1E+05	118538	88484	66652	43994	27302	15744	0
mean	178369	167013	1E+05	118444	92779	67918	43796	27456	16043	0
SD	2570	314	1548	165	3983	1184	241	147	264	0

From Table 2, the calibration curve was obtained, as shown in figure 24:

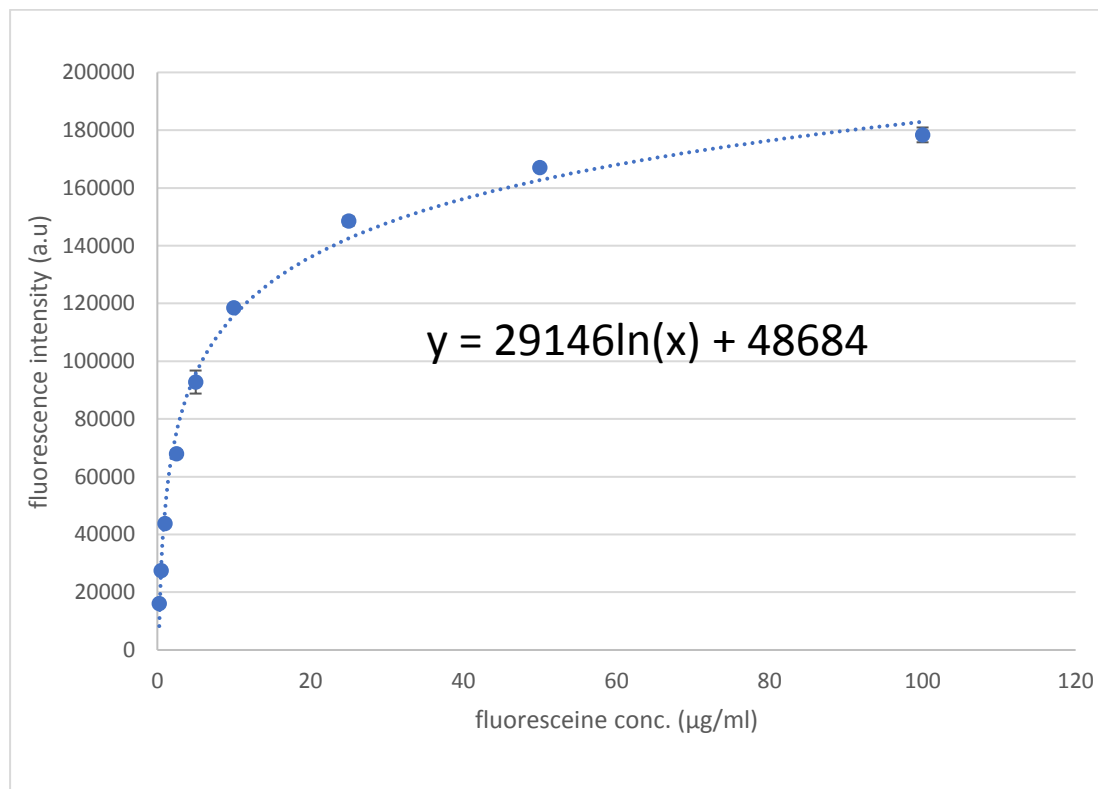


Figure 23: Calibration curve. Y: fluorescein intensity, X: fluorescein concentration

Equation 25 was obtained by linear regression analysis and describes the relation between the fluorescence intensity and fluorescein concentration as follows:

$$y = 29146 \ln(x) + 48684 \quad \text{Equation 24}$$

y: fluorescence intensity (a.u).

x: fluorescein concentration (µg/mL).

The fluorescein intensities for respective chips outlets and flow rates were determined by pipetting 100 μL of the samples to a 96-well plate, and repeated for every outlet (outlet 1, outlet 2, outlet 3, outlet 4, outlet 5) and flow rate (100 $\mu\text{L}/\text{min}$, 80 $\mu\text{L}/\text{min}$, 60 $\mu\text{L}/\text{min}$, 40 $\mu\text{L}/\text{min}$, 20 $\mu\text{L}/\text{min}$, 10 $\mu\text{L}/\text{min}$, 5 $\mu\text{L}/\text{min}$, 1 $\mu\text{L}/\text{min}$, 0,5 $\mu\text{L}/\text{min}$) for every chip (30 μm height, 45 μm height, 90 μm height), as shown in figure 25-c.

Table 3: Fluorescein intensity values of (30 μm) height chip.

Flow rates ($\mu\text{L}/\text{min}$)	Outlet 1 (a.u)	Outlet 2 (a.u)	Outlet 3 (a.u)	Outlet 4 (a.u)	Outlet 5 (a.u)
100	178825	179972	154766	25277	99217
80	174340	176602	156244	8982	5398
60	176756	177658	146283	34261	24430
40	178551	177537	161797	53022	2901
20	174268	176259	156759	52308	30034
10	180763	179613	164811	81081	5672
5	175739	162305	174930	99195	78426
1	179166	158130	105	129179	75655
0.5	1791	174973	70	71952	73544

Table 4: Fluorescein intensity values of (45 μm) height chip.

Flow rates ($\mu\text{L}/\text{min}$)	Outlet 1 (a.u)	Outlet 2 (a.u)	Outlet 3 (a.u)	Outlet 4 (a.u)	Outlet 5 (a.u)
100	170711	173491	168149	67501	4331
80	170789	170687	161077	64164	4826
60	171841	171411	166648	105936	13754
40	177894	174559	168236	71778	3925
20	173019	172670	163210	116339	8584
10	170000	170412	162021	72	10590
5	170567	166551	162237	118664	18754
1	167597	162975	49	115062	74
0.5	166530	68	1648	134363	51

Table 5: Fluorescein intensity values of (90 μm) height chip.

Flow rates ($\mu\text{L}/\text{min}$)	Outlet 1 (a.u)	Outlet 2 (a.u)	Outlet 3 (a.u)	Outlet 4 (a.u)	Outlet 5 (a.u)
100	165640	168713	163620	112475	14931
80	174337	169754	113264	95933	1294
60	171037	165824	120652	51881	2373
40	173746	169236	116717	21890	9318

20	173385	170981	166230	140077	7993
10	166271	162668	130614	76856	2861
5	162044	159462	126202	92600	4068
1	170740	159755	134623	131463	52431
0.5	161633	114	128860	101	72821

By replacing every value in these Tables by (y) in equation 24, the fluorescein concentration values were obtained.

4.6 SIMULATION OF THE MICROFLUIDIC GRADIENT GENERATOR

Simulation is the mimicry of process or performance of a real-world system [52].

4.6.1 Computational fluid dynamics:

Computational fluid dynamics (CFD) is a section of fluid mechanics which uses numerical analysis and data structures to find a solution and analyze cases related fluid flows [53].

4.6.2 Simulation process:

- Build geometry model [54].
- Mesh or grid: a network which is established of subdomains cells and points, used to solve multiple small equations [55]. For example, to simulate the fluid flows, it is difficult to simulate the whole flows at one, so the flow domains are divided to multi subdomains, and the subdomains can be simulated individually [56]. Mesh split up the geometry to small volumes which make it easier to calculate and simulate the different properties for this volume.
- Apply boundary conditions [54].
- Computational analysis [54].
- Visualization and results [54].

Note: the first three steps have been obtained by GAMBIT, while the last two steps can by FLUENT.

4.6.3 GAMBIT

GAMBIT is an abbreviation for Geometry And Mesh Building Intelligent Toolkit. It has a single interface to build a geometry and mesh it and these are the Fluent's preprocessing technologies[57]. The Gambit interface and its GUI components are shown in figure 24:

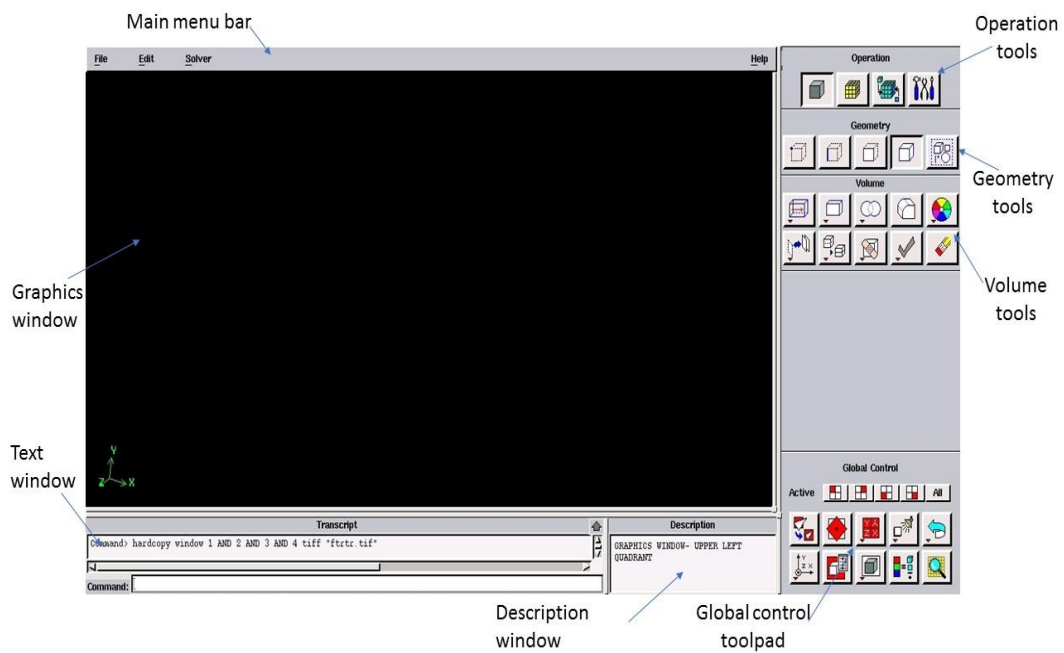


Figure 24: Gambit interface and GUI components

General sequence for designing geometry in Gambit:

- **Initial setup:** choose the solver type, and here the solver Fluent 5/6 is used [58].
- **Geometry designing and meshing:** Gambit has four types of geometries, and every geometry design start with these: vertices (x,y,z locations), edge (2 or more vertices), face (closed set of edges, 3 or more edges) and volume (closed set of faces, 4 or more faces). The best and easiest way to design is to start with 2-D geometry then sweep it to 3-D geometry with different depths (30 μm , 45 μm , 90 μm , 250 μm , 500 μm). To begin the 2-D geometry, the whole geometry is decomposed into different faces. For example, this random geometry in figure 25 can be decomposed into 5 faces. 1, 3, 5 are rectangular faces and 2, 4 are square faces.

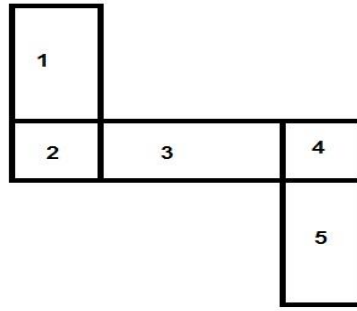


Figure 25: Random geometry as an example

This method is used for the whole geometry and at the end, the faces should be connected using the "connect faces" command in the face sub tools [58].

After checking that all faces are connected, the mesh can be applied. The quantity of meshes for the 2-D geometry is about 5879 meshes. After obtaining the 2-D meshed geometry, the meshed geometry is saved, so it can be used to generate the 3-D geometry. This can be done by creating an edge from any vertex, the edge length is the depth of the 3-D geometry (i.e. for the 3-D geometry with 30 μm depth, the edge length is 30 μm and for the 3-D geometry with 45 μm depth, the edge length is 45 μm , and so on for depths 30, 90, 250, 500 μm). then this edge is meshed. after that, all the faces are swept and meshed with the direction and path of the edge. So the 3-D meshed geometry is obtained [58]. The quantity of meshes for the 3-D geometry depends on the height of the geometry (for height 30 μm the quantity is 9788 meshes, for height 45 μm the quantity is 10894 meshes, for height 90 μm the quantity is 12745 meshes, for height 250 μm the quantity is 15847 meshes, for height 500 μm the quantity is 21874 meshes).

Note: all the dimensions here are in (mm), and they will be scaled later in Fluent to (mm), so at the end the dimensions will be in (μm). because there are no micrometer scales in CFD.

- **Mesh examination:** check the meshing.
- **Zone assignment:** define boundary conditions of the whole geometry, select which face is inlet1 and which face is inlet2 and

define inlet1, inlet2 as velocity inlets. And select which face is outlet1, outlet2, outlet3, outlet4, outlet5 and define them as pressure outlet, as shown in figure 26:

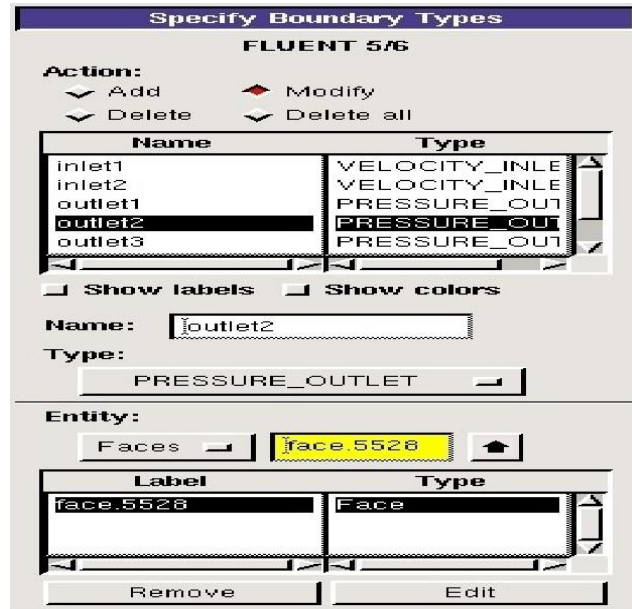


Figure 26: specify boundary types

- **export the mesh and save the geometry:**
Geometry saved as (*.dbs) file, Mesh is saved as (*.msh) file.

At the end, the 3-D geometry is obtained as shown in figure 27:

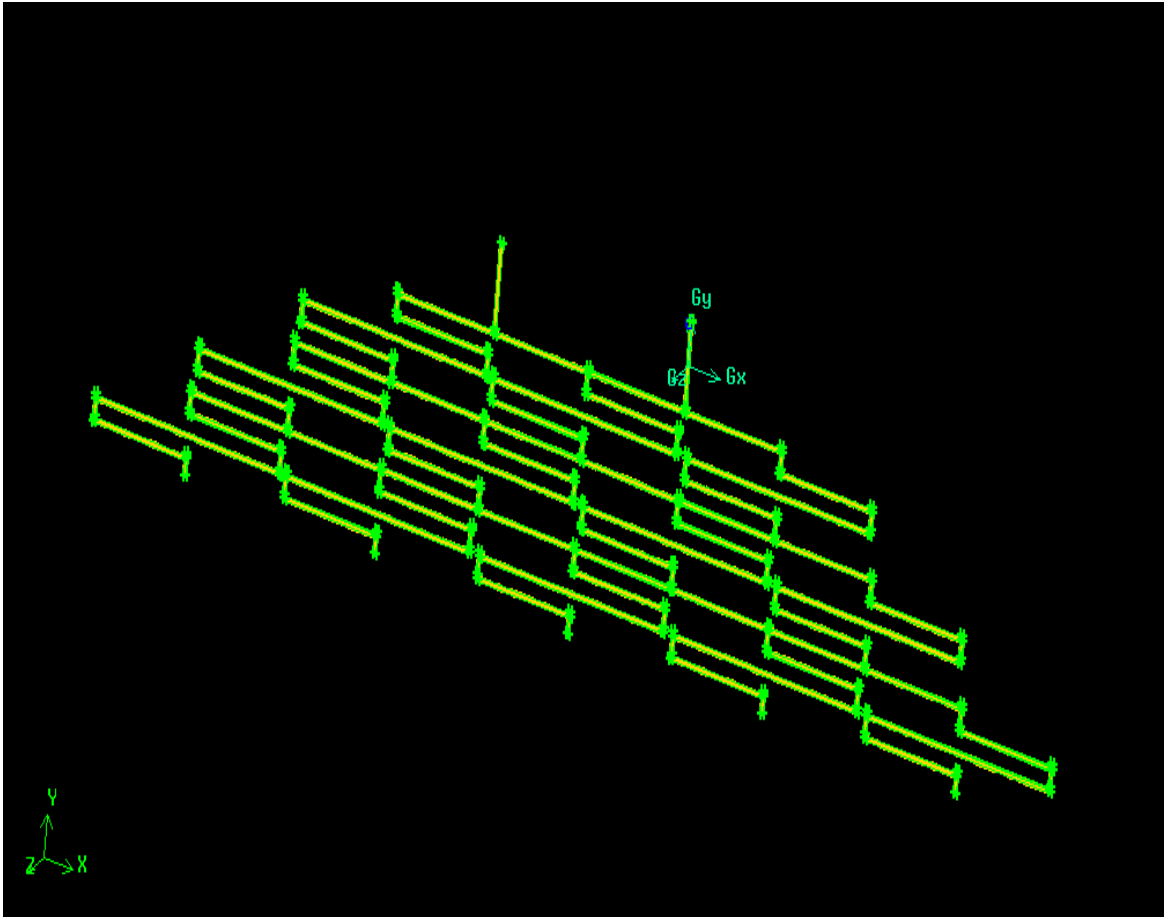


Figure 27: 3-D meshed geometry in Gambit.

4.6.4 Fluent

This CFD solver can handle both structured grids, i.e. rectangular grids with clearly defined node indices, and unstructured grids. Unstructured grids are generally of triangular nature, but can also be rectangular. In 3-D problems, unstructured grids can consist of tetrahedrals (pyramid shape), rectangular boxes, prisms, etc.

Note: the fluid in this simulation is laminar flow (as mentioned earlier in Reynolds number section), and the fluid flow state is steady (independent of time).

The general sequence of the operation:

First, the meshed geometry with the suffix (.msh) was loaded by using the command (file → read → case → file name.msh), then the loaded file was checked by using the command (Grid → check), then the geometry dimensions were scaled to mm (the geometry dimensions in Gambit were in mm, which means that the Fluent will handle the geometry as μm scale geometry) by using

the command (Grid → scale → change length units to mm), as shown in figure 28:

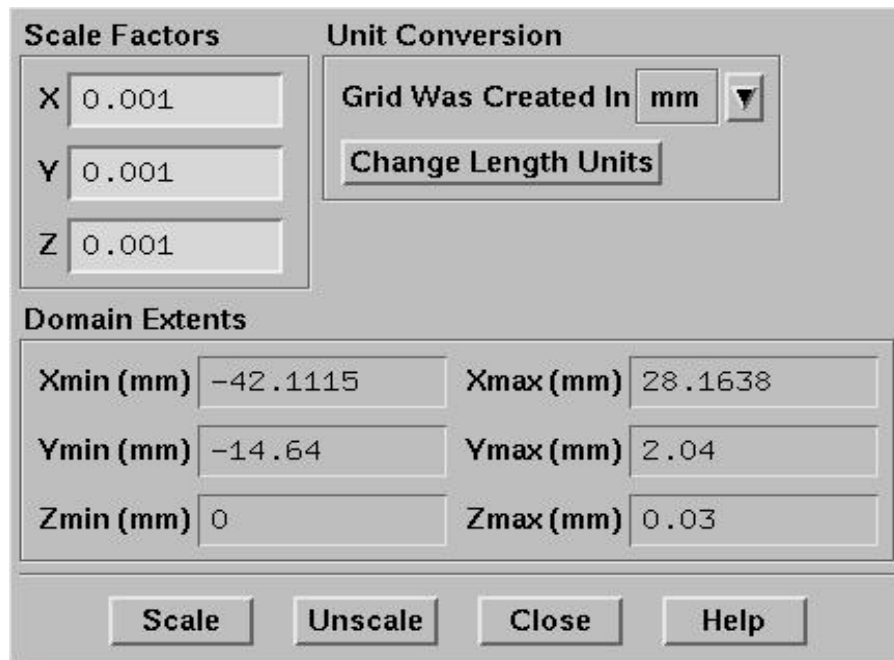


Figure 28: Length unit scaling

After dimensions scaling, the fluorescein (reagent) was defined and created, which is liquid water + fluorescein (nominal concentration of fluorescein in water is 1 g/L) by using the command (Models → species → transport and reaction → choose species transport in model).

Note: the energy equation will enable after this procedure, and it should be disabled.

Then the fluorescein creating was resumed by using the command (Define → material → material type choose fluid → fluent database → choose liquid water(h2o) then copy it → define fluorescein → make a mixture of fluorescein and water, as shown in figure (29,a) → define the density, Cp, thermal conductivity and viscosity as shown in figure (29,b) → define mass diffusivity of the mixture, as shown in figure (29,c,d):

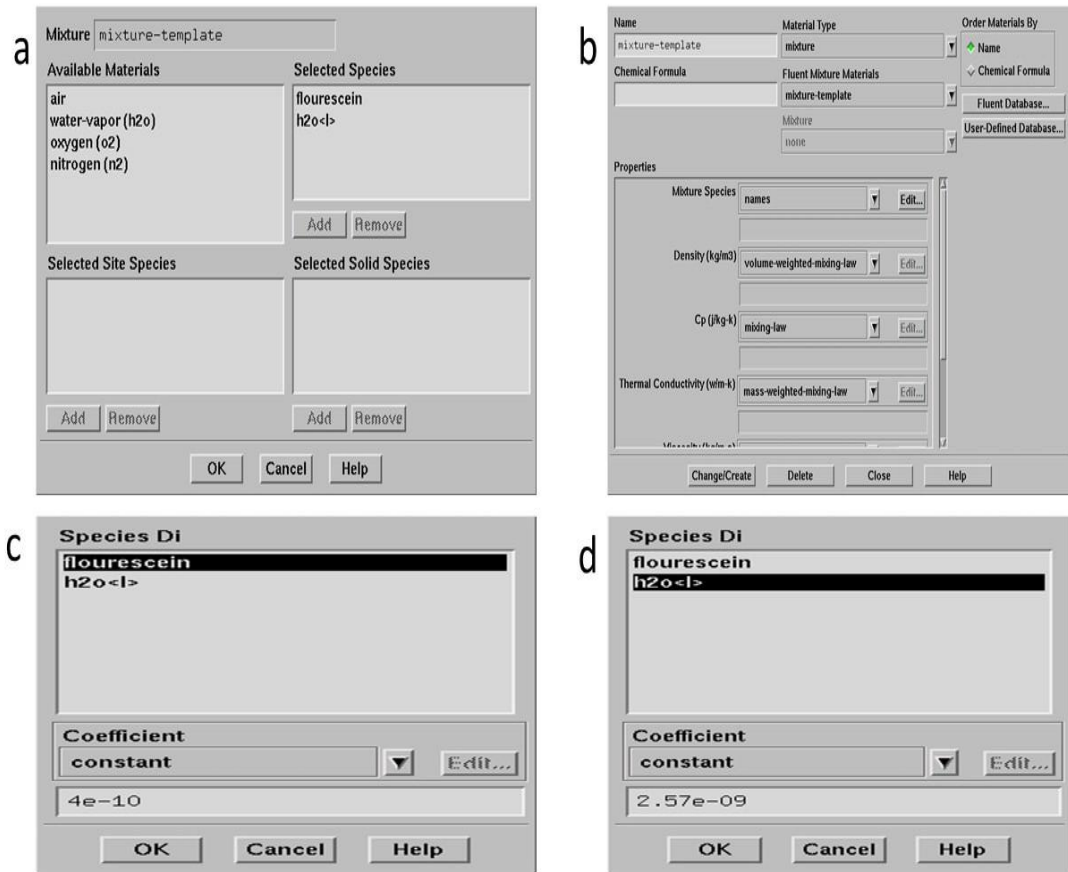


Figure 29: fluorescein and liquid water mixture define

Note: mass diffusivity of fluorescein = $4 \cdot 10^{-9} \text{ m}^2/\text{s}$, mass diffusivity of water = $2,57 \cdot 10^{-9} \text{ m}^2/\text{s}$.

Then the boundary conditions were defined which means defining the velocity in inlet 1, inlet 2 and the liquids by using the command (Define → boundary conditions → inlet1 → change velocity inlet, as shown in figure (30, a) → set velocity magnitude, as shown in figure (30, b) → set species mass friction to 0.001 (fluorescein concentration in the mixture), as shown in figure (30, c).

Note: for inlet 2, the velocity magnitude was just defined, which is the same as in inlet 1.

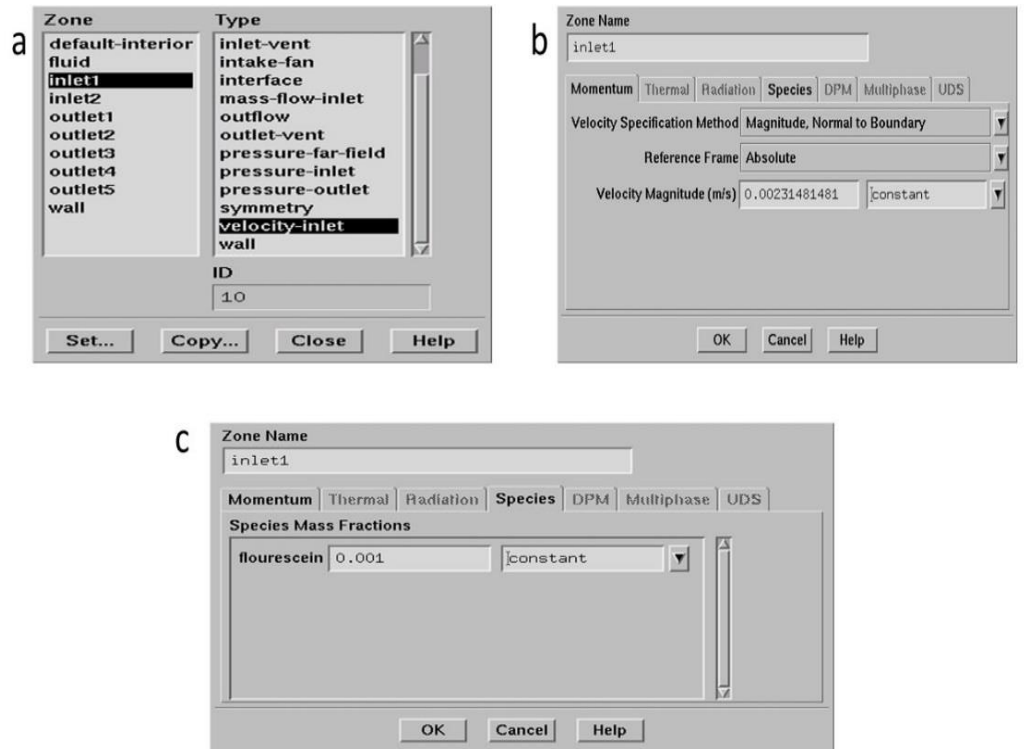


Figure 30: Boundary conditions define.

The velocities through the inlets can be calculated from equation 5:

$$Q = V \cdot A$$

This equation can be applied for different flow rates (100, 80, 60, 40, 20, 10, 5, 1, 0.5 $\mu\text{l}/\text{min}$) and different inlet areas for different heights (30, 45, 90, 250, 500 μm), and the table 6 was obtained:

Table 6: velocities through the inlets for different flow rates and different chips heights.

flow rate ($\mu\text{l}/\text{min}$)	Geometry depth (μm)				
	30 (m/s)	45 (m/s)	90 (m/s)	250 (m/s)	500 (m/s)
100	0.2319	0.1543	0.0772	0.027	0.0138
80	0.1852	0.1234	0.0617	0.0216	0.01104
60	0.1389	0.0926	0.0463	0.0162	0.00828
40	0.0926	0.0617	0.0309	0.0108	0.00552
20	0.0463	0.0309	0.0154	0.0054	0.00276
10	0.0231	0.0154	0.0077	0.0027	0.00138

5	0.0116	0.0077	0.0039	0.00135	0.00069
1	0.00231	0.0015	0.0008	0.00027	0.00014
0.5	0.00116	0.00077	0.0004	0.00014	0.00007

After defining the velocities through the inlets, the discretization for pressure, momentum, and fluorescein are changed as shown in figure 31:

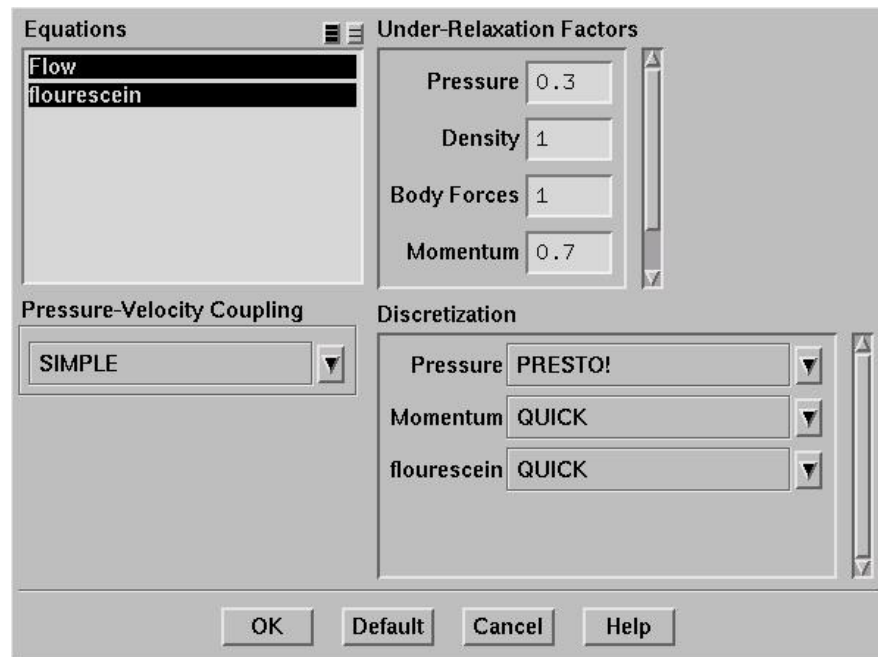


Figure 31: Discretization settings

Then, the residual monitors and surface monitors were defined as shown in figure 32 (a, b):

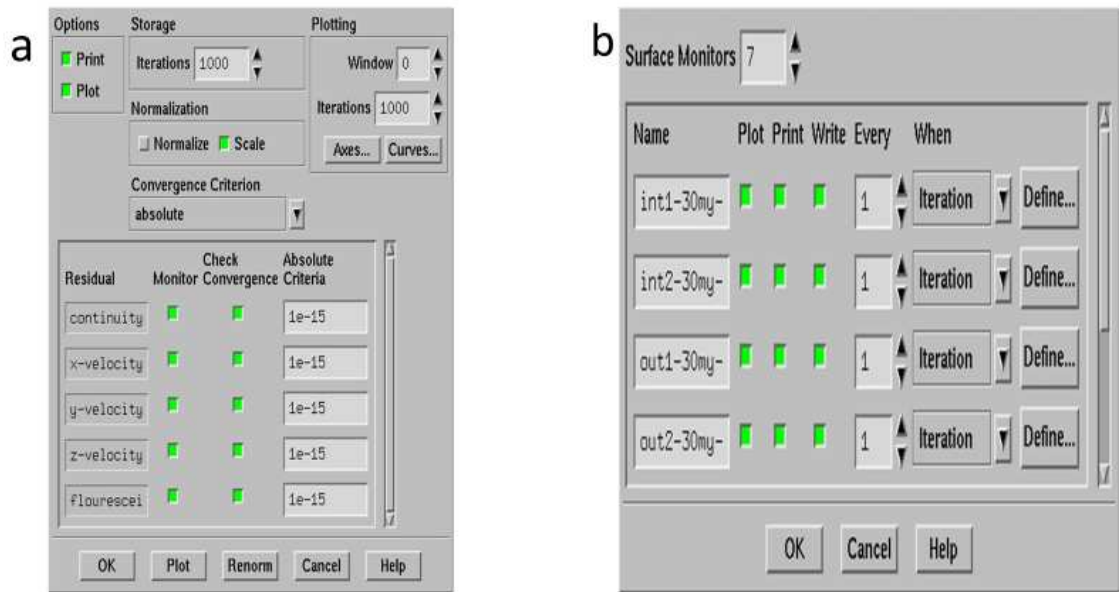


Figure 32: Residual and surface monitors.

Finally, the initialize was selected and the simulation started by selecting the Iterate command (300 iterates). This simulation took several hours to be done.

5 RESULTS AND DISCUSSION

5.1 GRAVIMETRIC RESULTS

To evaluate the flow through distribution of two solutes regarding different flow rates and heights (30 μl , 45 μl , 90 μl), total liquid volumes of the 5 individual outlets were collected and measured. The results were compared for individual flow rates with respect to volume loss. The results were presented according to the chips heights as follows:

- **30 μm height chip:**

Table 7: Gravimetric results of the (30 μm) height chip.

Flow rates ($\mu\text{l}/\text{min}$)	Outlet 1 (g)	Outlet 2 (g)	Outlet 3 (g)	Outlet 4 (g)	Outlet 5 (g)	Total (g)
100	0.1793	0.1927	0.1944	0.1751	0.1127	0.8542
80	0.1998	0.2092	0.2103	0.1895	0.1365	0.9453

60	0.2180	0.2265	0.2465	0.2159	0.1483	1.0552
40	0.2088	0.2196	0.2485	0.2113	0.1463	1.0345
20	0.1561	0.2246	0.2216	0.2014	0.1082	0.9119
10	0.1587	0.2363	0.2444	0.2287	0.1028	0.9709
5	0.1799	0.2848	0.2028	0.1655	0.1454	0.9784
1	0.3995	0.0518	0	0.1425	0.1974	0.7912
0.5	0.1868	0.2864	0	0	0.0657	0.5389

At first, the weights results were converted to volumes ($1 \mu\text{l} = 0.001 \text{ g}$). In an ideal situation, the liquid compound in every outlet should be $200 \mu\text{l}$ with a total volume that was infused through the chip of $1000 \mu\text{l}$ evenly distributed over five outlets. For high flow rates of $100 \mu\text{l}/\text{min}$ down to $5 \mu\text{l}/\text{min}$, the results in outlets (1 & 5) are less than expected because they are far from the center and liquid will travel more distance that means more blocks, the driven pressure became less and chances for bubbles creation are increased. In contrast, the volume in outlets (3, 4, 5) are approximate as expected.

For low flow rates of $1 \mu\text{l}/\text{min}$ and $0.5 \mu\text{l}/\text{min}$, the results were not as expected. Even outlet (3) at a flow rate ($1 \mu\text{l}/\text{min}$) has no liquid, and outlets (3 & 4) at a flow rate ($0.5 \mu\text{l}/\text{min}$) have no liquid compound.

It can be considered that at low flow rates ($1 \mu\text{l}/\text{min}$, $0.5 \mu\text{l}/\text{min}$), the liquid volumes distribution is not efficient. The deviations in both cases are mainly caused by air bubble formation due to the permeable properties of PDMS. Liquid evaporation inside the PDMS channels and ambient temperature were also factors that affect the flow dynamics. Emerging bubble results in high interfacial tension and resistance and they cannot be washed out at low flow regimes. Also, the liquid in the silicon Tygon tubes can potentially be lost during the measurement in the pipette tips and in Eppendorf tubes again due to evaporation. Figures 33, 34, 35 are showing liquid compound weight at every outlet and at multiple flow rates for the ($30 \mu\text{m}$) height chip.

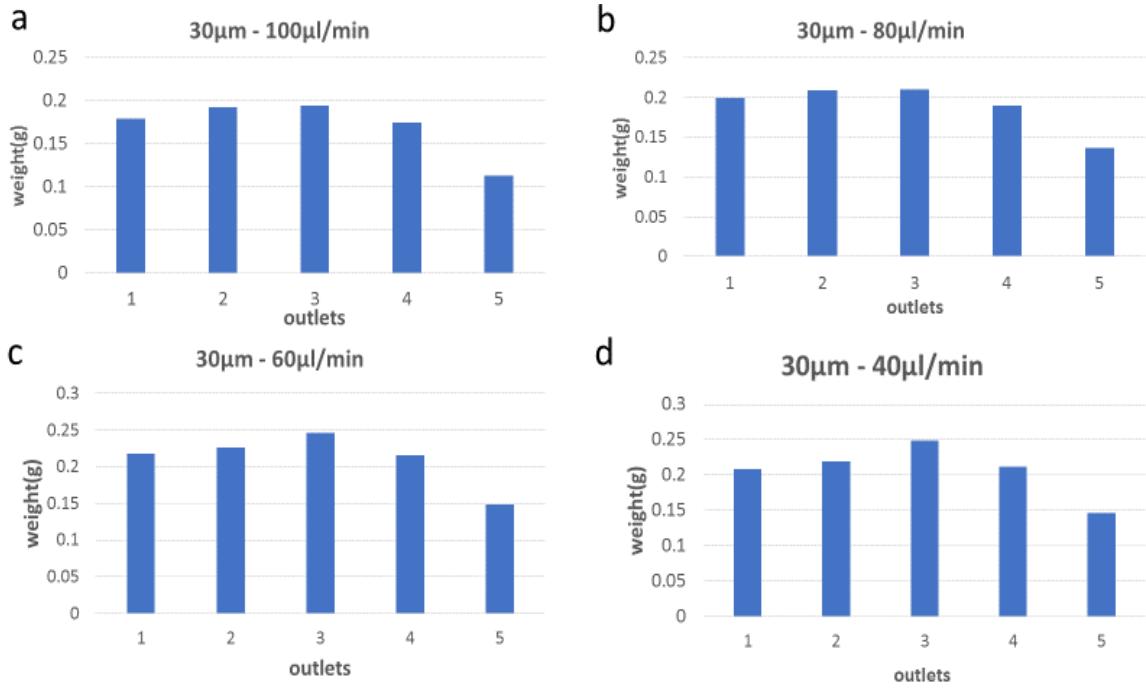


Figure 33: a) The liquid compound weights at every outlet for (30 μm) height chip at a flow rate (100 μl/min). b) The liquid compound weights at every outlet for (30 μm) height chip at a flow rate (80 μl/min). c) The liquid compound weights at every outlet for (30 μm) height chip at a flow rate (60 μl/min). d) The liquid compound weights at every outlet for (30 μm) height chip at a flow rate (40 μl/min).

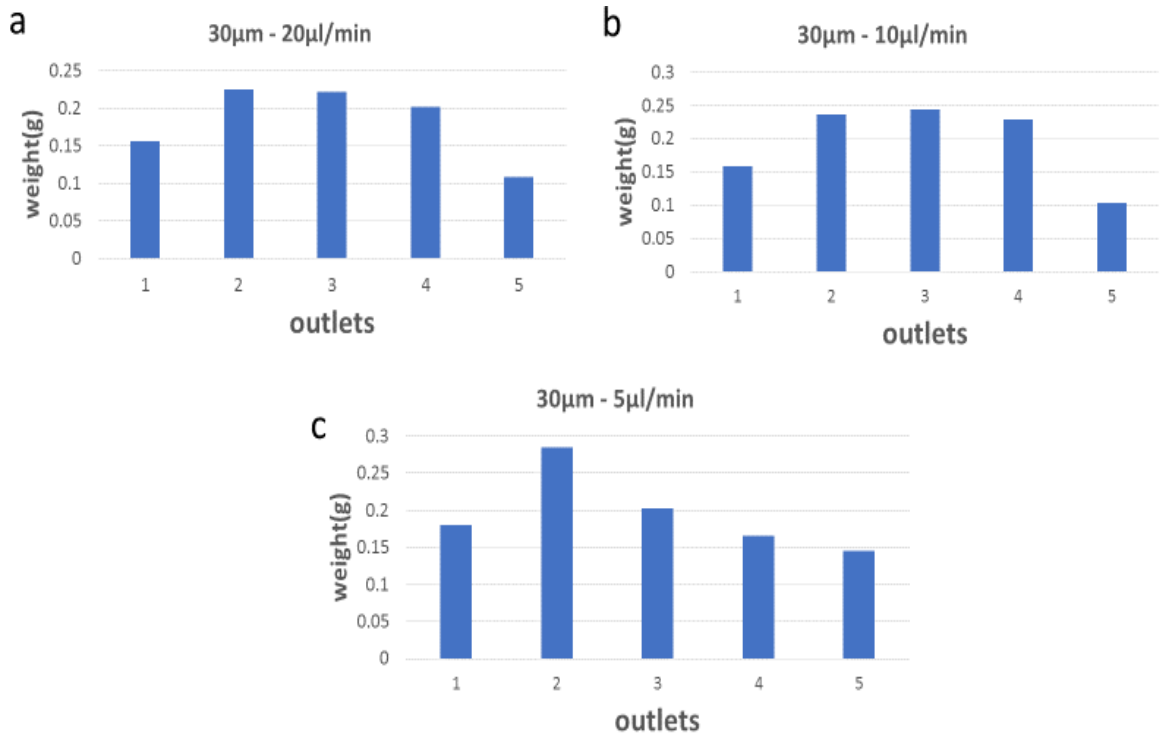


Figure 34: a) The liquid compound weights at every outlet for (30 µm) height chip at a flow rate (20 µl/min). b) The liquid compound weights at every outlet for (30 µm) height chip at a flow rate (10 µl/min). c) The liquid compound weights at every outlet for (30 µm) height chip at a flow rate (5 µl/min).

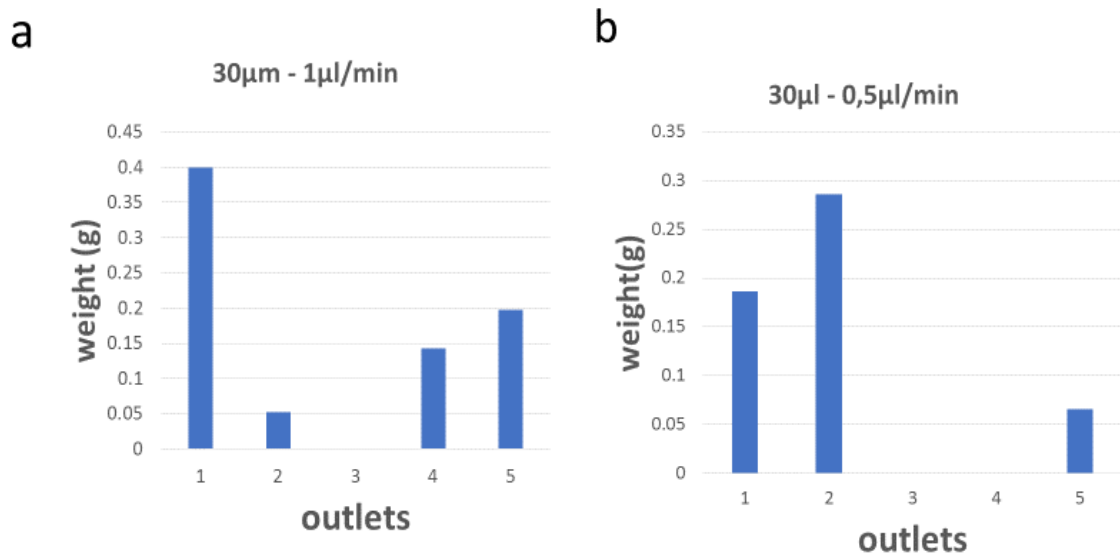


Figure 35: a) The liquid compound weights at every outlet for (30 µm) height chip at a flow rate (1 µl/min). b) The liquid compound weights at every outlet for (30 µm) height chip at a flow rate (0.5 µl/min).

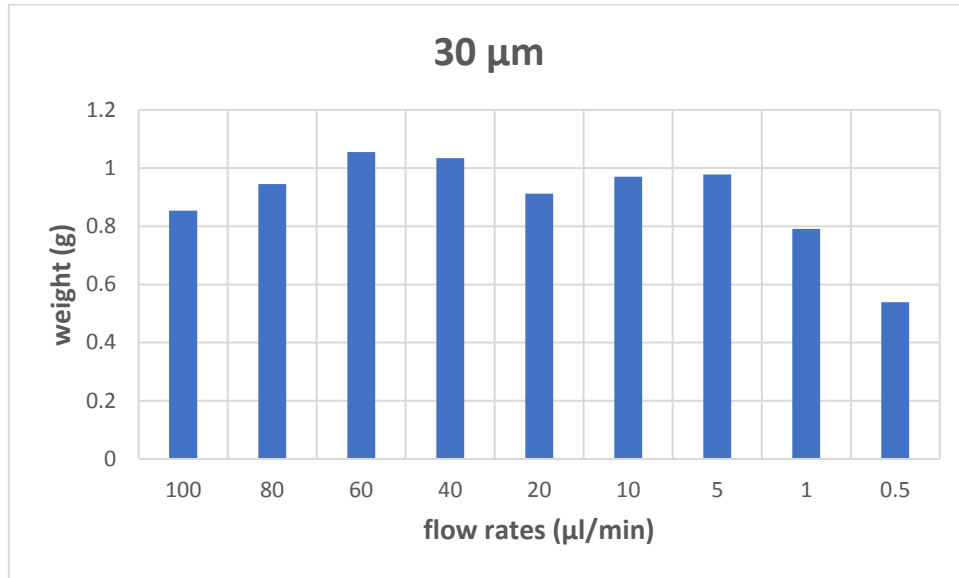


Figure 36: Comparison of the liquid compound total weight at each different flow rate of (30 μm) height chip.

As seen in Figure 36, the flow rate has an impact on the gravimetric results indicated by the relative standard deviation (RSD) of 17.6% between the total weights of individual outlets.

- **45 μm height chip:**

Table 8: Gravimetric results of the (45 μm) height chip.

Flow rates (μl/min)	Outlet 1 (g)	Outlet 2 (g)	Outlet 3 (g)	Outlet 4 (g)	Outlet 5 (g)	Total (g)
100	0.1546	0.2068	0.1870	0.2368	0.1820	0.9672
80	0.1689	0.1992	0.1983	0.2160	0.1732	0.9556
60	0.1427	0.2028	0.2017	0.2119	0.1807	0.9398
40	0.1432	0.2398	0.2068	0.2438	0.1833	1.0169
20	0.1335	0.2166	0.1631	0.2786	0.0810	0.8728
10	0.1478	0.1973	0.1638	0.2313	0.1688	0.909
5	0.3282	0.3172	0.0905	0.2160	0.1024	1.0543
1	0.2551	0.4833	0	0.0556	0	0.794
0.5	0.7734	0	0.0111	0.0706	0	0.8551

In Table 8, it can be noted the absence of the liquid in outlet 3 and outlet 5 at a flow rate of 1 μl/min and also in outlet 2 and outlet 5 at flow rate 0.5 μl/min again due to bubble

formation. The liquid volume distribution is still good at high flow rates (100 $\mu\text{l}/\text{min}$, 80 $\mu\text{l}/\text{min}$, 60 $\mu\text{l}/\text{min}$, 40 $\mu\text{l}/\text{min}$, 20 $\mu\text{l}/\text{min}$, 10 $\mu\text{l}/\text{min}$, 5 $\mu\text{l}/\text{min}$). Figures 37, 38 and 39 are showing liquid compound weight at every outlet and at multiple flow rates for the (45 μm) height chip.

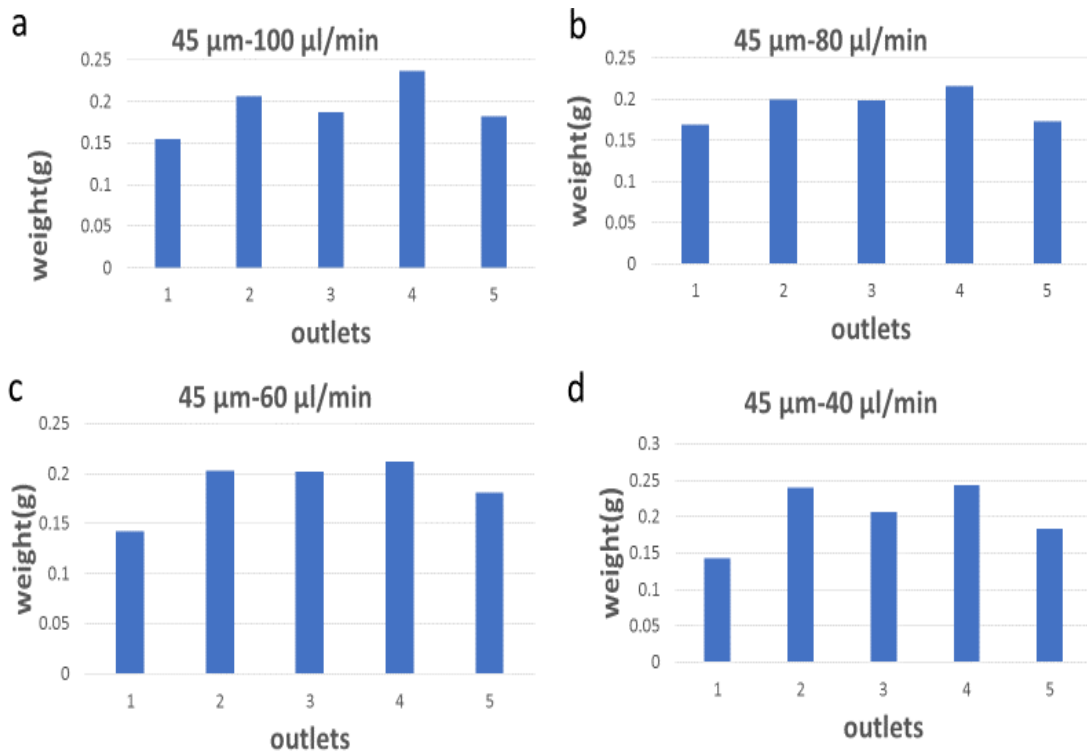


Figure 37: a) The liquid compound weights at every outlet for (45 μm) height chip at a flow rate (100 $\mu\text{l}/\text{min}$). b) The liquid compound weights at every outlet for (45 μm) height chip at a flow rate (80 $\mu\text{l}/\text{min}$). c) The liquid compound weights at every outlet for (45 μm) height chip at a flow rate (60 $\mu\text{l}/\text{min}$). d) The liquid compound weights at every outlet for (45 μm) height chip at a flow rate (40 $\mu\text{l}/\text{min}$).

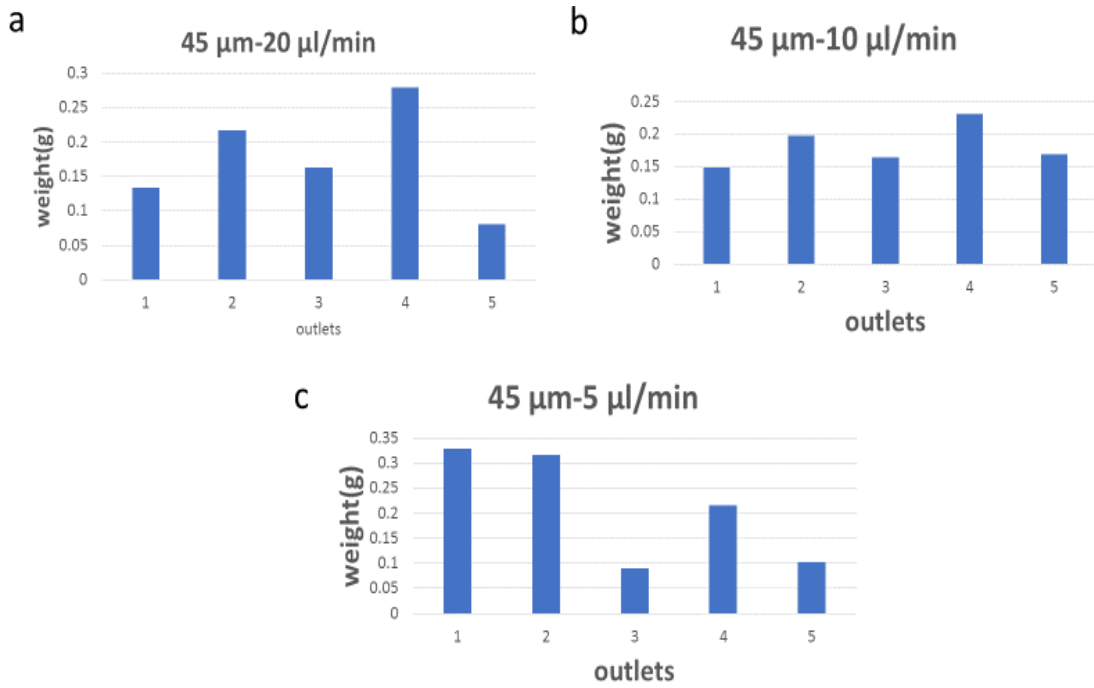


Figure 38: a) The liquid compound weights at every outlet for (45 µm) height chip at a flow rate (20 µl/min). b) The liquid compound weights at every outlet for (45 µm) height chip at a flow rate (10 µl/min). c) The liquid compound weights at every outlet for (45 µm) height chip at a flow rate (5 µl/min).

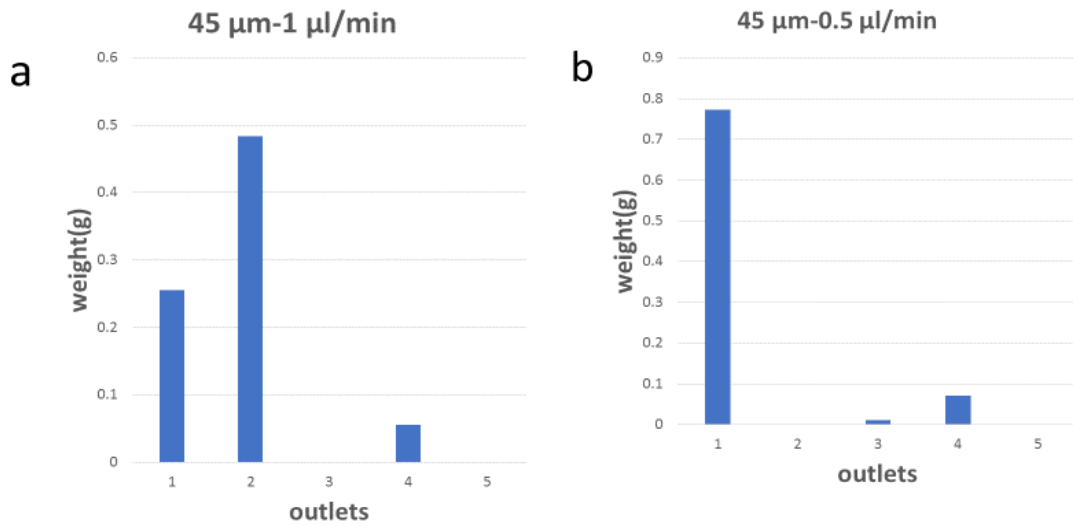


Figure 39: a) The liquid compound weights at every outlet for (45 µm) height chip at a flow rate (1 µl/min). b) The liquid compound weights at every outlet for (45 µm) height chip at a flow rate (0,5 µl/min).

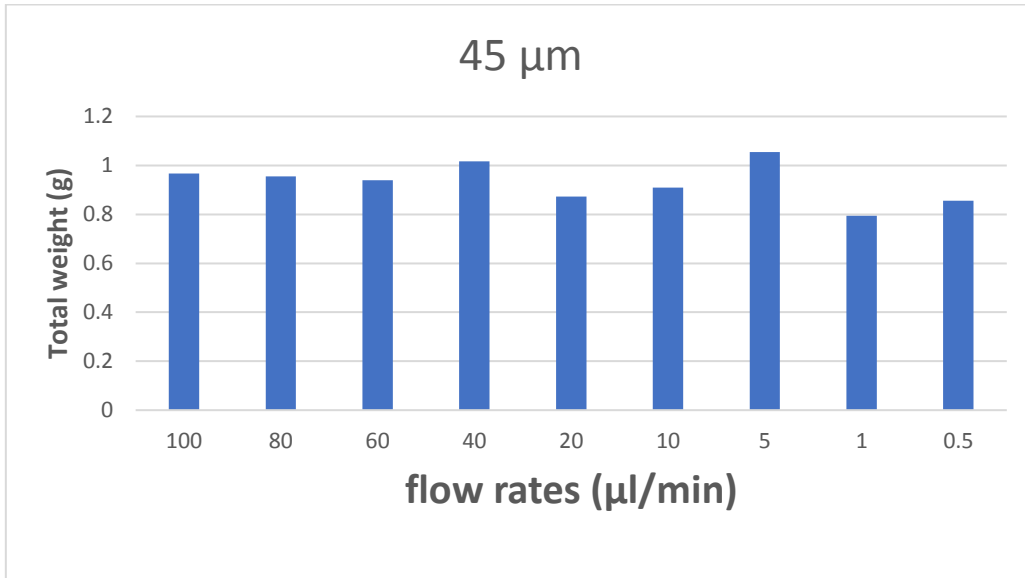


Figure 40: Comparison of the liquid compound total weight at each different flow rate of (45 μm) height chip.

As seen in Figure 40, the flow rate has an impact on the gravimetric results indicated by the relative standard deviation (RSD) of 8.75% between the total weights of individual outlets and the increase in height results in more evenly distributed total volumes compared to 30 μm channels.

- **90 μm height chip:**

Table 9: Gravimetric results of the 90 μm chip.

Flow rates (μl/min)	Outlet 1 (g)	Outlet 2 (g)	Outlet 3 (g)	Outlet 4 (g)	Outlet 5 (g)	total (g)
100	0.1659	0.2372	0.154	0.1698	0.2284	0.9553
80	0.2114	0.0544	0.186	0.2128	0.295	0.9596
60	0.1925	0.2529	0.2104	0.1682	0.259	1.083
40	0.1411	0.1967	0.2187	0.1013	0.327	0.9848
20	0.0942	0.3018	0.3367	0.1029	0.138	0.9736
10	0.011	0.0689	0.5266	0.2934	0.0605	0.9604
5	0.0556	0.2241	0.3674	0.1961	0.1419	0.9851
1	0.1858	0.2068	0.28	0.1465	0.0351	0.8542
0.5	0.2569	0	0.3915	0	0.0632	0.7116

In Table 9, it can be noted that there was absence of the compound liquid in outlet 2 and outlet 4 at flow rate (0.5 μl/min). The liquid volume distribution is still good at high flow rates (100 μl/min, 80 μl/min, 60 μl/min, 40 μl/min, 20 μl/min, 10 μl/min, 5 μl/min), and it still once again inhomogenous at low flow rates (1 μl/min, 0.5 μl/min), as in the previous

chips for similar reasons. The Figures 41, 42, 43 are showing liquid compound weight at every outlet and at multiple flow rates for the (90 μm) height chip:

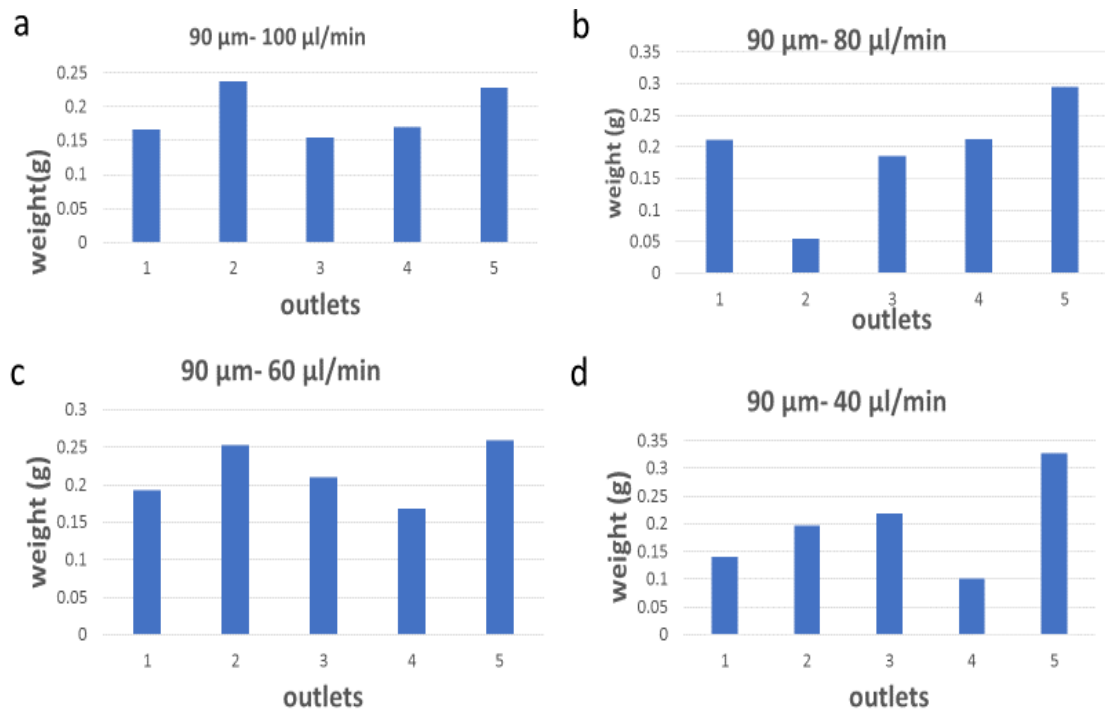


Figure 41: a) The liquid compound weights at every outlet for (90 μm) height chip at flow rate (100 $\mu\text{l}/\text{min}$). b) The liquid compound weights at every outlet for (90 μm) height chip at flow rate (80 $\mu\text{l}/\text{min}$). c) The liquid compound weights at every outlet for (90 μm) height chip at flow rate (60 $\mu\text{l}/\text{min}$). d) The liquid compound weights at every outlet for (90 μm) height chip at flow rate (40 $\mu\text{l}/\text{min}$).

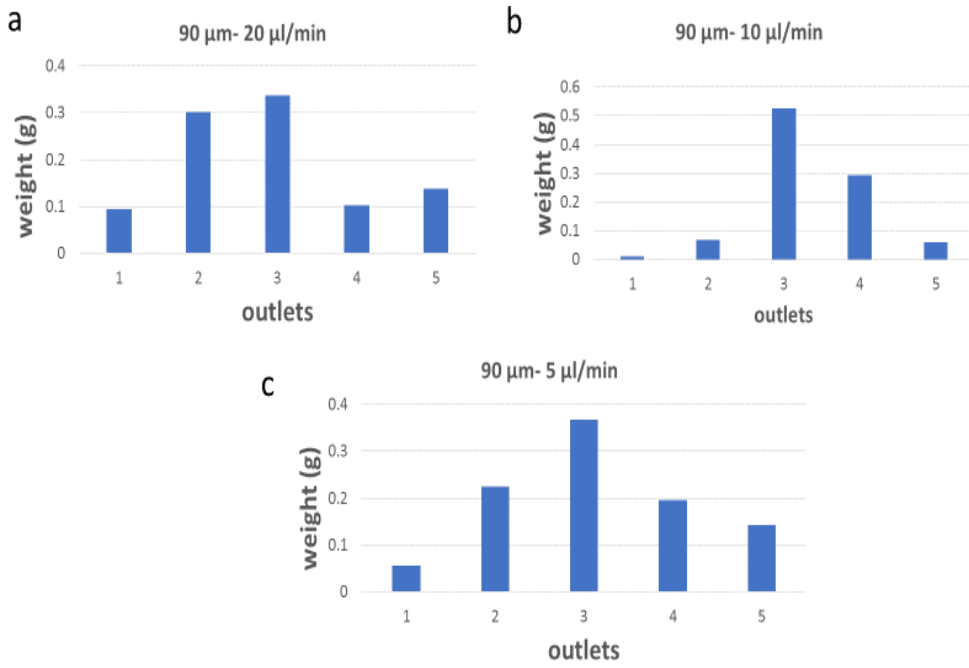


Figure 42: a) The liquid compound weights at every outlet for (90 μm) height chip at a flow rate (20 μl/min). b) The liquid compound weights at every outlet for (90 μm) height chip at a flow rate (10 μl/min). c) The liquid compound weights at every outlet for (90 μm) height chip at a flow rate (5 μl/min).

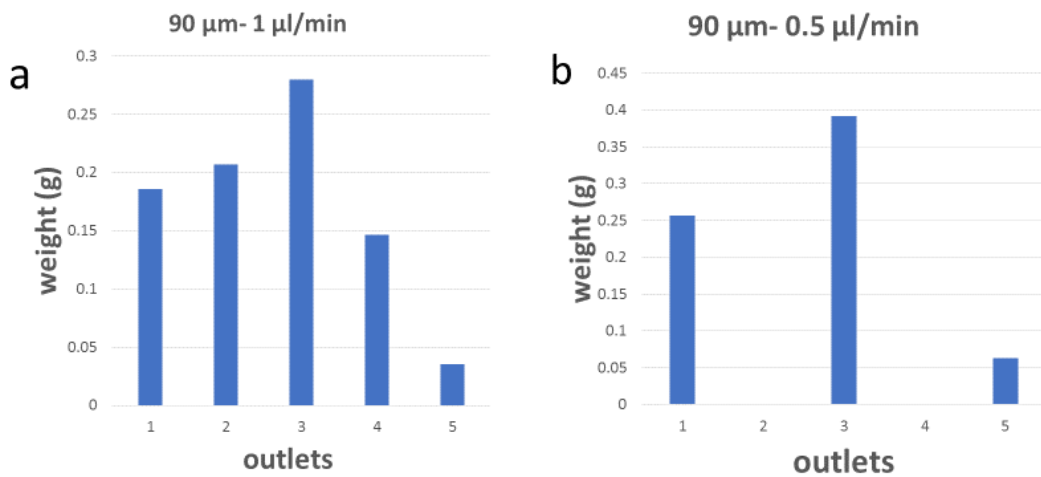


Figure 43: a) The liquid compound weights at every outlet for (90 μm) height chip at a flow rate (1 μl/min). b) The liquid compound weights at every outlet for (90 μm) height chip at a flow rate (0,5 μl/min).

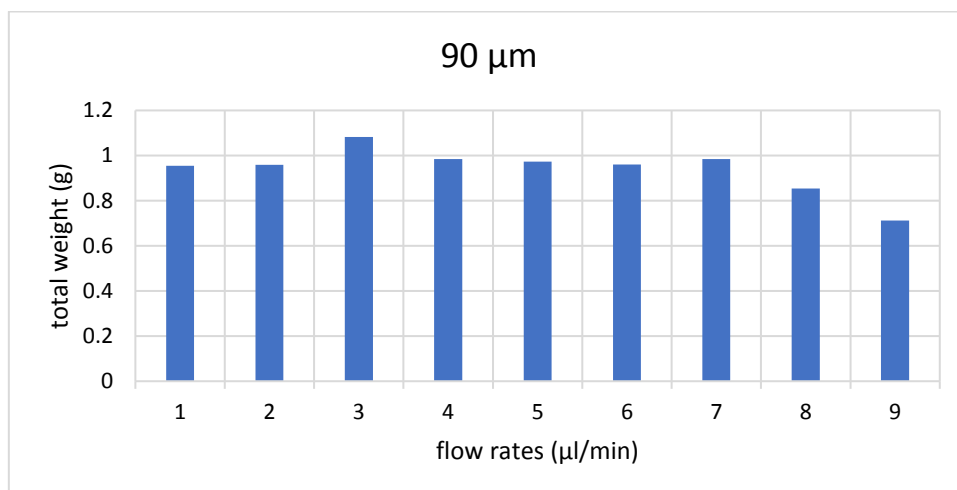


Figure 44: Comparison of the liquid compound total weight at each different flow rate of (90 μm) height chip.

As seen in Figure 44, the flow rate has an impact on the gravimetric results indicated by the relative standard deviation (RSD) of 11.03 % between the total weights of individual outlets.

Overall, for 30 μm height chip at high flow rates (100 μl/min, 80 μl/min, 60 μl/min, 40 μl/min) the results were accepted (taking into consideration the small deviation from the expected result for every outlet). At medium flow rates (20 μl/min, 10 μl/min, 5 μl/min), the differences between the outlets are beginning to be noticeable and the deviation from the expected result for specific outlets is large, caused by factors and restrictions that mentioned before. At low flow rates (1 μl/min, 0.5 μl/min), the difference between the outlets are clearly noticeable and the deviation from the expected result for specific outlets is larger than higher flow rates, caused by factors and restrictions that mentioned before. For 45 μm height chip, the fluid flow velocity is lower than the previous chip, the differences between the outlets are beginning to be noticeable at high flow rates (40 μl/min) with a similar performance for the lowest flow rates.

For 90 μm high chip, the fluid flow velocity is lower than the previous two chips, the differences between the outlets are beginning to be noticeable at higher flow rates than the previous two chips. Same goes for medium and low flow rates similar to previous two chip heights, however, overall transported volumes were best and most homogenous over the selected flow rate range even though fluid velocity is lower compared to the other chip heights.

5.2 ON-CHIP GENERATION OF FLUORESCHEIN SODIUM SALT

To evaluate the fluorescein concentration of the liquid compound in every outlet in regards to different flow rates and heights (30 μm , 45 μm , and 90 μm). The results are presented consecutively according to the chips heights:

- **30 μm height chip:**

Table 10: Fluorescein concentration results at different flow rates of 30 μm height chip.

flow rates ($\mu\text{l}/\text{min}$)	outlet 1 ($\mu\text{g}/\text{ml}$)	outlet 2 ($\mu\text{g}/\text{ml}$)	outlet 3 ($\mu\text{g}/\text{ml}$)	outlet 4 ($\mu\text{g}/\text{ml}$)	outlet 5 ($\mu\text{g}/\text{ml}$)
100	86.933	90.423	38.08	0.44794	5.6621
80	74.534	80.549	40.06	0.2561	0.22647
60	80.976	83.521	28.464	0.60966	0.43511
40	86.12	83.175	48.468	1.1605	0.20788
20	74.35	79.607	40.774	1.1324	0.52735
10	92.91	89.316	53.749	3.039	0.22861
5	78.199	49.32	76.059	5.6578	2.7744
1	58.955	42.737	0.18885	15.827	2.5227
0.5	0.18881	71.837	0.18883	0.18887	14.259

- **45 μm height chip:**

Table 11: Fluorescein concentration results at different flow rates of 45 μm height chip.

flow rates ($\mu\text{l}/\text{min}$)	outlet 1 ($\mu\text{g}/\text{ml}$)	outlet 2 ($\mu\text{g}/\text{ml}$)	outlet 3 ($\mu\text{g}/\text{ml}$)	outlet 4 ($\mu\text{g}/\text{ml}$)	outlet 5 ($\mu\text{g}/\text{ml}$)
100	65.809	72.395	60.271	1.9072	0.21833
80	65.985	65.754	47.286	1.7008	0.22207
60	68.41	67.408	57.245	7.13	0.30166
40	84.2	75.097	60.451	2.2086	0.21531
20	71.232	70.384	50.876	10.188	0.25263
10	64.223	65.137	48.842	0.18865	0.2763
5	65.484	57.055	49.206	11.034	0.35812
1	58.326	49.772	0.1859	9.6173	0.18606

0.5	56.229	0.18602	0.19639	18.649	0.18592
------------	--------	---------	---------	--------	---------

- **90 μm height chip:**

Table 12: Fluorescein concentration results at different flow rates of 90 μm height chip.

flow rates ($\mu\text{l}/\text{min}$)	outlet 1 ($\mu\text{g}/\text{ml}$)	outlet 2 ($\mu\text{g}/\text{ml}$)	outlet 3 ($\mu\text{g}/\text{ml}$)	outlet 4 ($\mu\text{g}/\text{ml}$)	outlet 5 ($\mu\text{g}/\text{ml}$)
100	55.299	61.448	51.597	8.9233	0.31409
80	74.527	63.683	53.237	5.0587	0.19672
60	66.549	55.650	41.813	1.1159	0.20414
40	73.031	62.561	57.381	0.3988	0.25907
20	72.132	66.421	56.430	23.005	0.24756
10	56.510	49.939	46.627	2.6289	0.20759
5	48.881	44.737	44.291	4.5121	0.21637
1	65.874	45.189	42.079	17.118	1.1372
0.5	48.196	0.18892	55.656	0.18883	2.2891

5.3 SIMULATION RESULTS FOR FLUORESCIN SODIUM SALT

To evaluate the CFD simulation results of fluorescein concentration of the liquid compound in every outlet in regards to different flow rates and heights (30 μm , 45 μm , 90 μm , 250 μm , and 500 μm). The results are presented according to the chips heights as follows:

- **30 μm height chip:**

Table 13: Simulation of Fluorescein concentration results at different flow rates for 30 μm height chip.

flow rates ($\mu\text{l}/\text{min}$)	outlet 1 ($\mu\text{g}/\text{ml}$)	outlet 2 ($\mu\text{g}/\text{ml}$)	outlet 3 ($\mu\text{g}/\text{ml}$)	outlet 4 ($\mu\text{g}/\text{ml}$)	outlet 5 ($\mu\text{g}/\text{ml}$)
100	100	97.9391	50.0698	1.93	9.28E-06
80	100	97.8776	50.0843	2	9.93E-06
60	100	97.7606	50.1053	2.11	1.04E-05
40	100	97.5409	50.1518	2.32	1.07E-05
20	100	96.9338	50.1807	2.94	1.08E-05
10	100	95.7375	50.1512	4.18	1.14E-05
5	100	93.4474	50.0995	6.52	1.13E-05

1	100	76.3521	50.0198	23.485	1.02E-05
0.5	100	77.7602	50.0232	22.3009	1.25E-05

- **45 μm height chip:**

Table 14: Simulation of Fluorescein concentration results at different flow rates for 45 μm height chip.

flow rates ($\mu\text{l}/\text{min}$)	outlet 1 ($\mu\text{g}/\text{ml}$)	outlet 2 ($\mu\text{g}/\text{ml}$)	outlet 3 ($\mu\text{g}/\text{ml}$)	outlet 4 ($\mu\text{g}/\text{ml}$)	outlet 5 ($\mu\text{g}/\text{ml}$)
100	99.99999	97.74693	50.09566	2.165067	9.77E-06
80	99.99993	97.69615	50.0696	2.23166	9.49E-06
60	99.99999	97.55644	50.05916	2.358528	9.14E-06
40	99.99999	97.27247	50.10841	2.636444	9.83E-06
20	99.99999	96.36375	50.12367	3.557328	1.03E-05
10	99.99999	94.54625	50.0933	5.419201	1.01E-05
5	99.99999	91.20693	50.06073	8.793979	1.07E-05
1	99.99999	79.00837	50.01657	21.05727	1.02E-05
0.5	99.99999	76.64708	50.03011	23.40738	1.03E-05

- **90 μm height chip:**

Table 15: Simulation of Fluorescein concentration results at different flow rates for 90 μm height chip.

flow rates ($\mu\text{l}/\text{min}$)	outlet 1 ($\mu\text{g}/\text{ml}$)	outlet 2 ($\mu\text{g}/\text{ml}$)	outlet 3 ($\mu\text{g}/\text{ml}$)	outlet 4 ($\mu\text{g}/\text{ml}$)	outlet 5 ($\mu\text{g}/\text{ml}$)
100	100	97.08815	49.99175	2.904927	9.56E-06
80	100	97.015	49.98571	2.971741	9.05E-06
60	100	96.75398	49.98262	3.212511	4.81E-06
40	100	96.15233	49.99835	3.822614	0
20	100	94.19642	50.03205	5.780174	1.01E-05
10	100	90.64094	50.03247	9.353113	9E-06
5	100	85.37599	50.01038	14.67136	1.01E-05
1	100	76.55004	50.03058	23.50392	1.03E-05
0.5	100	76.34551	50.03073	23.70829	8.78E-06

- **250 μm height chip:**

Table 16: Simulation of Fluorescein concentration results at different flow rates for 250 μm height chip.

flow rates ($\mu\text{l}/\text{min}$)	outlet 1 ($\mu\text{g}/\text{ml}$)	outlet 2 ($\mu\text{g}/\text{ml}$)	outlet 3 ($\mu\text{g}/\text{ml}$)	outlet 4 ($\mu\text{g}/\text{ml}$)	outlet 5 ($\mu\text{g}/\text{ml}$)
100	100	94.9926	50.0162	5.05	1.01E-05
80	100	94.493	95	5.52	1.01E-05
60	100	93.5952	50.0277	6.43	9.51E-06
40	100	91.8183	50.0282	8.19	8.92E-06
20	100	87.2614	50.0166	12.7603	9.78E-06
10	100	81.642	50.0224	18.4034	9.74E-06
5	100	77.5667	50.0297	22.4865	1.03E-05
1	100	76.3396	50.0307	23.7142	9.47E-06
0.5	100	76.3395	50.0307	23.7142	7.57E-06

- **500 μm height chip:**

Table 17: Simulation of Fluorescein concentration results at different flow rates for 500 μm height chip.

flow rates ($\mu\text{l}/\text{min}$)	outlet 1 ($\mu\text{g}/\text{ml}$)	outlet 2 ($\mu\text{g}/\text{ml}$)	outlet 3 ($\mu\text{g}/\text{ml}$)	outlet 4 ($\mu\text{g}/\text{ml}$)	outlet 5 ($\mu\text{g}/\text{ml}$)
100	100	92.8065	50.0235	7.19	0
80	100	91.7178	50.0279	8.27	8.97E-06
60	100	90.0429	50.0653	9.94	7.96E-06
40	100	87.1947	50.0375	12.8196	9.53E-06
20	100	81.684	50.0259	18.3588	9.7E-06
10	100	77.62	50.0299	22.4327	9.37E-06
5	100	76.4131	50.0307	23.6405	9.73E-06
1	100	76.3368	50.0307	23.717	7.82E-06
0.5	100	76.3368	50.0307	23.717	6.53E-06

After determination of fluorescein concentration in Tables (13- 17), it can be summarized that

- The mixing resolution thus fluorescein concentration distribution is perfect in outlet1, outlet3 and outlet5 for every chip (30 μm , 45 μm , 90 μm , 250 μm , 500 μm) and at every flow rate (100 $\mu\text{l}/\text{min}$, 80 $\mu\text{l}/\text{min}$, 60 $\mu\text{l}/\text{min}$, 40 $\mu\text{l}/\text{min}$, 20 $\mu\text{l}/\text{min}$, 10 $\mu\text{l}/\text{min}$, 5 $\mu\text{l}/\text{min}$, 1 $\mu\text{l}/\text{min}$, 0.5 $\mu\text{l}/\text{min}$).

- The mixing resolution of the fluorescein concentration distribution is not perfect in outlet2 and outlet4 for chips with channel heights of 30 μm , 45 μm and 90 μm at high flow rates (100 $\mu\text{l}/\text{min}$, 80 $\mu\text{l}/\text{min}$, 60 $\mu\text{l}/\text{min}$, 40 $\mu\text{l}/\text{min}$, 20 $\mu\text{l}/\text{min}$, 10 $\mu\text{l}/\text{min}$, 5 $\mu\text{l}/\text{min}$). This caused by convection, which dominates at high velocities.
- The mixing resolution of the fluorescein concentration distribution enhanced and became better for chips with heights 30 μm , 45 μm , and 90 μm at the low flow rates (1 $\mu\text{l}/\text{min}$, 0.5 $\mu\text{l}/\text{min}$).
- For 250 μm height chip, the mixing resolution or the fluorescein concentration distribution enhanced and became better at flow rates (10 $\mu\text{l}/\text{min}$, 5 $\mu\text{l}/\text{min}$, 1 $\mu\text{l}/\text{min}$, 0.5 $\mu\text{l}/\text{min}$).
- For 500 μm height chip, the mixing resolution or the fluorescein concentration distribution enhanced and became better at flow rates (20 $\mu\text{l}/\text{min}$, 10 $\mu\text{l}/\text{min}$, 5 $\mu\text{l}/\text{min}$, 1 $\mu\text{l}/\text{min}$, 0.5 $\mu\text{l}/\text{min}$).
- The overall concentration range of the chip is dependent on the flow rate applied, thus flow velocity inside the microchannels. The velocity or flow rate is an important factor affecting the concentration gradient profile. The presented simulation results correspond well with already published results for similar gradient generator types with typical sigmoidal gradient curve shape [57] [19]. For comparison, the simulated concentration profiles of chips with similar heights (200 vs. 250 μm) were compared at velocity range of 0.001 m/s to 0.0001 m/s.

5.4 COMPARISON BETWEEN EXPERIMENTAL AND CFD SIMULATION FOR CONCENTRATION GRADIENT GENERATOR CHIPS

To evaluate and compare the experimental results of fluorescein concentration generation on-chip and the simulation results, the fluorescein concentration of the liquid compound in every outlet regarding different flow rates and heights (30 μm , 45 μm , 90 μm) was analyzed in the subsequent set of experiments.

Experimental results of the 30 μm high microfluidic gradient generators corresponded well with the CFD simulation results for flow rates in the range between 100 $\mu\text{l}/\text{min}$ and 10 $\mu\text{l}/\text{min}$ as shown in Figure 45. For lower flow rates of 5 to 0,5 $\mu\text{l}/\text{min}$ the concentration gradient of sodium fluorescein was inhomogeneous most probably again due to the

formation of bubbles and obstruction of individual channel outputs (e.g. output 1 and 3 of Figure 46i). The best agreement between the CFD simulation and the experimental results were obtained at a flow rate of 40 to 10 $\mu\text{l}/\text{min}$.

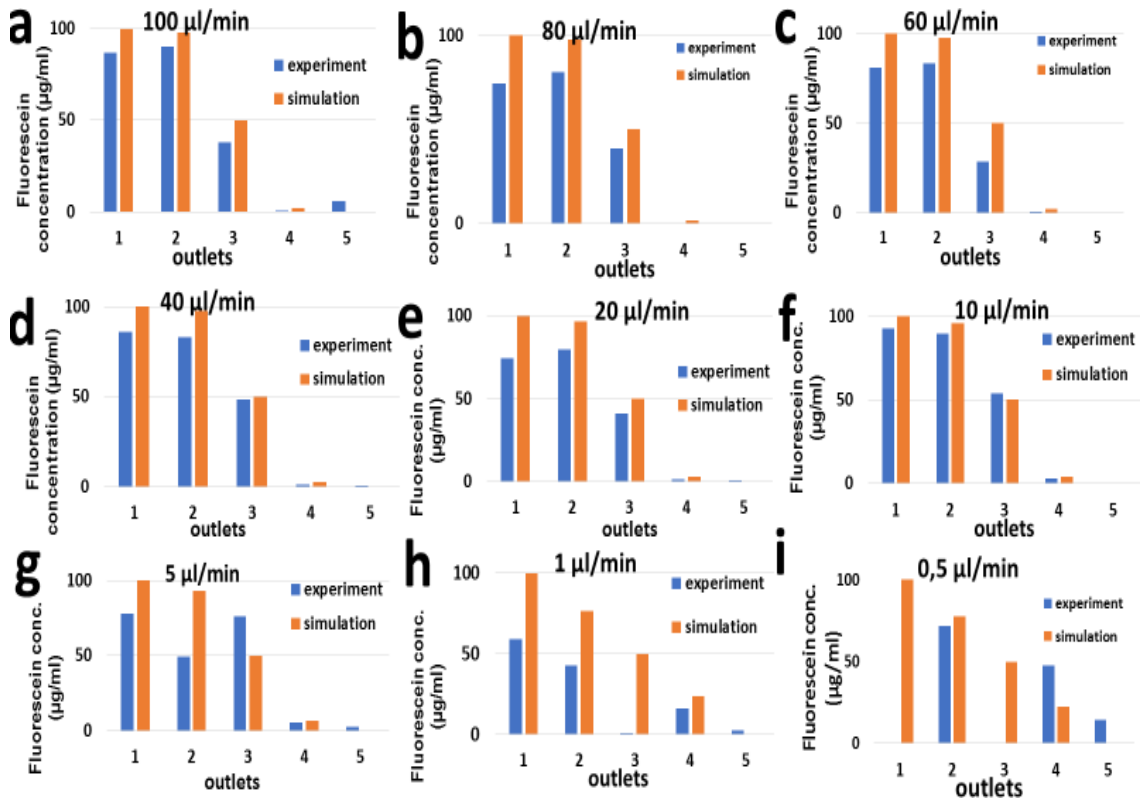


Figure 45: (a-i) Comparison between experimental data and CFD simulation results for 100 $\mu\text{g}/\text{ml}$ fluorescein sodium salt solution for 30 μm high microfluidic gradient generators.

Experimental results of the 45 μm height microfluidic gradient generators surprisingly revealed similar overall behavior compared to the smaller channel height for flow rates in the range between 100 $\mu\text{l}/\text{min}$ and 5 $\mu\text{l}/\text{min}$ as shown in Figure 46 indicating better performance for a slightly lower flow rate of 5 $\mu\text{l}/\text{min}$. For lower flow rates of 1 to 0,5 $\mu\text{l}/\text{min}$ the concentration gradient generators yielded again inhomogeneous due to evaporation, bubble growth and channel blockage (e.g. output 2 and 3 of Figure 46i). The best agreement between the CFD simulation and the experimental results were obtained at a flow rate of 40 $\mu\text{l}/\text{min}$, most linear gradient with a slower slope however at a flow rate of 5 $\mu\text{l}/\text{min}$.

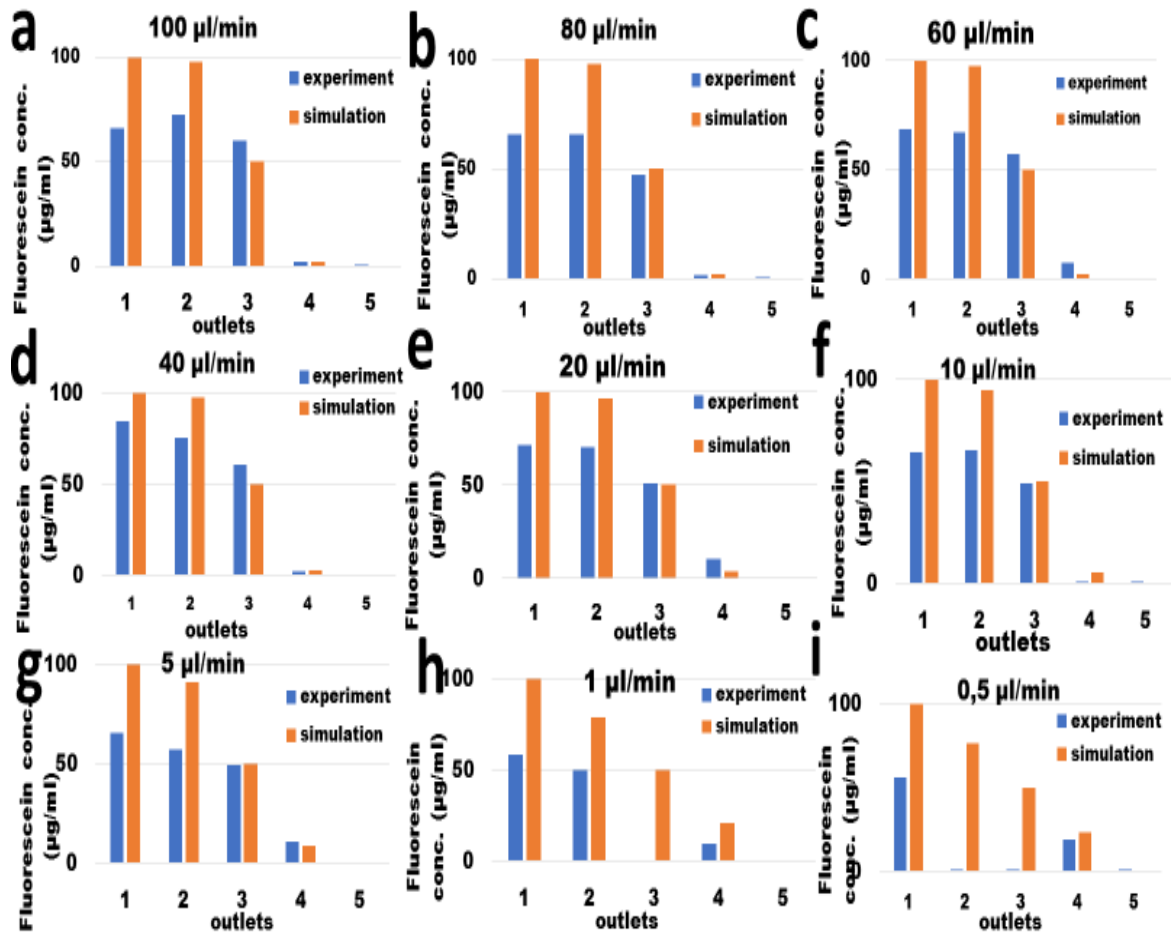


Figure 46: (a-i) Comparison between experimental data and CFD simulation results for 100 µg/ml fluorescein sodium salt solution for 45 µm high microfluidic gradient generators.

In a final experimental set-up, the performance of microfluidic gradient generators with 90 µm height microchannel was evaluated. Surprisingly as shown in Figure 47 similar overall behavior compared to both 30 and 45 µm height channels for flow rates in the range between 100 µl/min and 1 µl/min with an even better performance for a slightly lower flow rate of 1 µl/min as the 45 µm designs. For the lowest flow rate of 0,5 µl/min the concentration gradient generators yielded again inhomogeneous results comparable to the results showed before due to evaporation of liquid and bubble growth within the microchannels and channel blockage (e.g. output 2 and 4 of Figure 47i). The best agreement between the CFD simulation and the experimental results were obtained at a flow rate of 60-80 µl/min, most linear gradient with a slower slope however at a flow rate of 1 µl/min.

In contrast to the CFD simulation results of microchannels featuring perfect surface roughness and chemical homogeneity, in the experimental setup two different flow regimes could be identified: One higher flow regime for sigmoidal concentrations that corresponds very well with simulation results as well as data and simulations published in literature [57], at lower flow velocities also linear concentration gradients were achieved (e.g. 1 μ l-0.5 μ l/min for 30 μ m high microchannels as shown in Figure 45 h-i). Differences between the experiment results possibly are a result from differences in the roughness of microchannel, because with common photolithographic means it is difficult to ensure a very clean Nano-surface environment [57]. Similar behavior has been reported for alternative chip-based strategies for the creation of non-linear concentration gradients with the similar microchannel dimensions ($L=6$ mm, $W=400$ μ m, $h=30$ μ m) [58]. In particular, flow-based chips, where gradients are generated within a single y-shaped channel featuring linear micropatterns are accurate at low flow velocity and large diffusion coefficients [40]. Too high as well as too low flow rates below and above critical velocity range result in significant errors of the generated gradients.

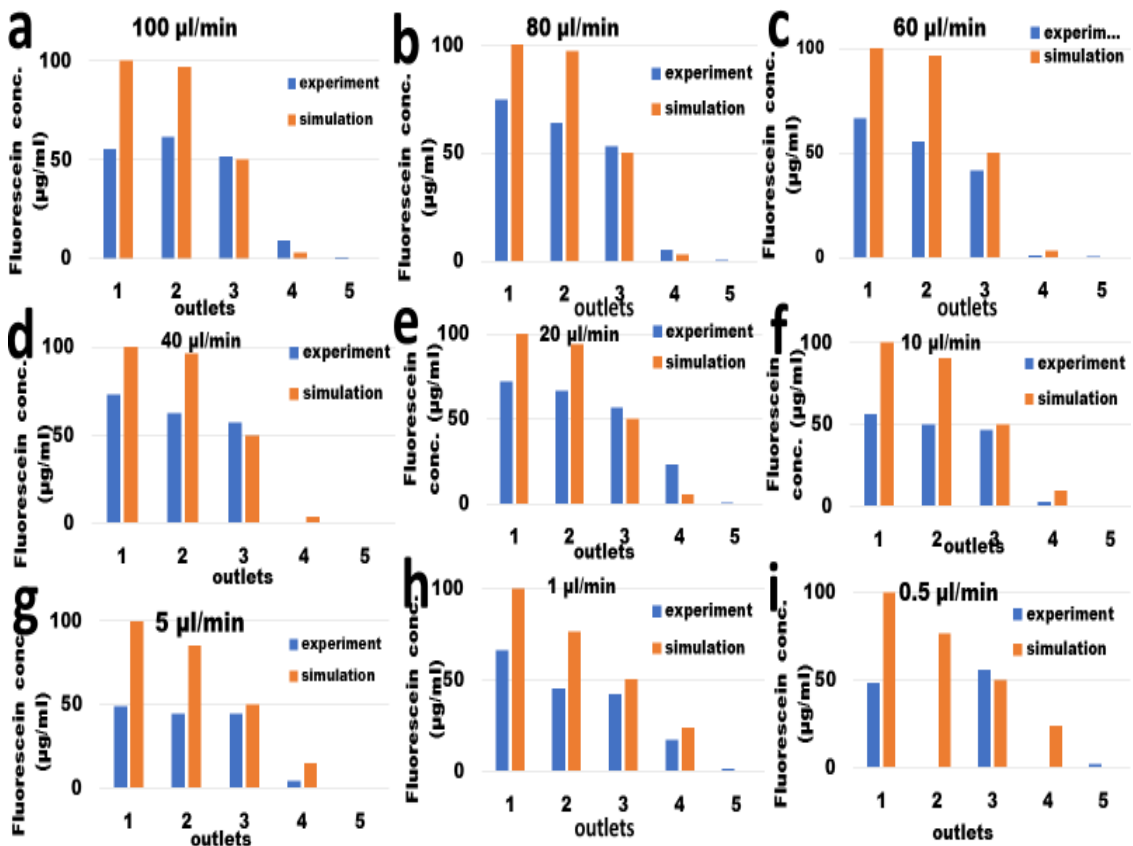


Figure 47: (a-i) Comparison between experimental data and CFD simulation results for 100 μ g/ml fluorescein sodium salt solution for 90 μ m high microfluidic gradient generators.

6 CONCLUSION

Concentration gradient generators can serve for multiple experiments since it increases the resolution of dose-response studies and reduces analysis time and other efforts. Selection of a particular gradient generator platform requires considering experimental needs, such as maintaining low shear forces while keep the medium continuous perfusion, maintaining in-vivo like conditions, retaining signal molecules and removing waste, etc. The microfluidic gradient generator could provide precise gradient control and gradient pattern. These applications include integration with multiplexed drug screening, organs-on-a-chip and some in other fields. The presented gradient generator platform can provide a microenvironment to investigate the miniaturized mammalian cell cultures and its response to chemical signals. Combined efforts would continue to benefit the field next few years to expand availability of these platforms and demonstrate their capabilities in a complex platform. CFD simulations are a valuable tool for design and initial performance evaluation of such micro engineered prototype systems. In general, it can be concluded that the mixing efficiency of the 30 μm height chip gives more reliable results than 45 and 90 μm height chips therefore a decrease of the chip height gives better mixing, in other words, a decrease in cross-section area led to an approximation to the respective simulation. The poor mixing results at high flow rates can be controlled by making the channels longer or increasing the microfluidic gradient generator chip levels. The best mixing results were obtained at low flow rates (1 $\mu\text{l}/\text{min}$, 0.5 $\mu\text{l}/\text{min}$), but at these flow rates, the blocking probabilities were higher than at high flow rates. For future applications, it has to be considered to balance between the flow rate and the chip height and the channel length.

7 REFERENCES

- [1] G. M. Whitesides, "The origins and the future of microfluidics," *Nature*, vol. 442, no. 7101, pp. 368–373, Jul. 2006.
- [2] C. Hu, J. Liu, H. Chen, and F. Nie, "Microfluidic Platforms for Gradient Generation and its Applications," *Biochemistry & Analytical Biochemistry*, vol. 06, no. 02, 2017.
- [3] D. Weibel and G. Whitesides, "Applications of microfluidics in chemical biology," *Current Opinion in Chemical Biology*, vol. 10, no. 6, pp. 584–591, Dec. 2006.
- [4] K. E. Nelson, J. O. Foley, and P. Yager, "Concentration Gradient Immunoassay. 1. An Immunoassay Based on Interdiffusion and Surface Binding in a Microchannel," *Analytical Chemistry*, vol. 79, no. 10, pp. 3542–3548, May 2007.
- [5] B. E. Root, M. L. Hammock, and A. E. Barron, "Thermoresponsive *N*-alkoxyalkylacrylamide polymers as a sieving matrix for high-resolution DNA separations on a microfluidic chip," *ELECTROPHORESIS*, vol. 29, no. 23, pp. 4677–4683, Dec. 2008.
- [6] L. L. Sohn, O. A. Saleh, G. R. Facer, A. J. Beavis, R. S. Allan, and D. A. Notterman, "Capacitance cytometry: Measuring biological cells one by one," *Proceedings of the National Academy of Sciences*, vol. 97, no. 20, pp. 10687–10690, Sep. 2000.
- [7] J. Kameoka, H. G. Craighead, H. Zhang, and J. Henion, "A Polymeric Microfluidic Chip for CE/MS Determination of Small Molecules," *Analytical Chemistry*, vol. 73, no. 9, pp. 1935–1941, May 2001.
- [8] P. Belgrader, M. Okuzumi, F. Pourahmadi, D. A. Borkholder, and M. A. Northrup, "A microfluidic cartridge to prepare spores for PCR analysis," *Biosens Bioelectron*, vol. 14, no. 10–11, pp. 849–852, Jan. 2000.
- [9] J. Yang, Y. Huang, X. B. Wang, F. F. Becker, and P. R. Gascoyne, "Cell separation on microfabricated electrodes using dielectrophoretic/gravitational field-flow fractionation," *Anal. Chem.*, vol. 71, no. 5, pp. 911–918, Mar. 1999.
- [10] D. T. Chiu *et al.*, "Patterned deposition of cells and proteins onto surfaces by using three-dimensional microfluidic systems," *Proceedings of the National Academy of Sciences*, vol. 97, no. 6, pp. 2408–2413, Mar. 2000.
- [11] "Researchers produce smallest ever 3D printed microfluidic 'lab on a chip' device," *3ders.org*. [Online]. Available: <http://www.3ders.org/articles/20170811-researchers-produce-smallest-ever-3d-printed-microfluidic-lab-on-a-chip-device.html>. [Accessed: 17-Nov-2018].
- [12] "LOC PCR - Lab on Chip PCR." [Online]. Available: <https://www.gene-quantification.de/lab-on-chip.html>. [Accessed: 29-Nov-2018].
- [13] A. Bernard, B. Michel, and E. Delamarche, "Micromosaic Immunoassays," *Analytical Chemistry*, vol. 73, no. 1, pp. 8–12, Jan. 2001.
- [14] A. G. G. Toh, Z. P. Wang, C. Yang, and N.-T. Nguyen, "Engineering microfluidic concentration gradient generators for biological applications," *Microfluidics and Nanofluidics*, vol. 16, no. 1–2, pp. 1–18, Jan. 2014.
- [15] J. M. Lee, J. Kim, E. Kang, S.-H. Lee, and B. G. Chung, "An integrated microfluidic culture device to regulate endothelial cell differentiation from embryonic stem cells," *ELECTROPHORESIS*, vol. 32, no. 22, pp. 3133–3137, Nov. 2011.

- [16] F. Wang *et al.*, “Microfluidic delivery of small molecules into mammalian cells based on hydrodynamic focusing,” *Biotechnology and Bioengineering*, vol. 100, no. 1, pp. 150–158, May 2008.
- [17] “1999_Nature_0.pdf.” .
- [18] X. Wang, Z. Liu, and Y. Pang, “Concentration gradient generation methods based on microfluidic systems,” *RSC Advances*, vol. 7, no. 48, pp. 29966–29984, 2017.
- [19] Y. Wang, T. Mukherjee, and Q. Lin, “Systematic modeling of microfluidic concentration gradient generators,” *Journal of Micromechanics and Microengineering*, vol. 16, no. 10, pp. 2128–2137, Oct. 2006.
- [20] H. Somaweera, A. Ibraguimov, and D. Pappas, “A review of chemical gradient systems for cell analysis,” *Analytica Chimica Acta*, vol. 907, pp. 7–17, Feb. 2016.
- [21] R. Milo and R. Phillips, *Cell biology by the numbers*. New York, NY: Garland Science, Taylor & Francis Group, 2016.
- [22] M. Meier, E. M. Lucchetta, and R. F. Ismagilov, “Chemical stimulation of the Arabidopsis thaliana root using multi-laminar flow on a microfluidic chip,” *Lab on a Chip*, vol. 10, no. 16, p. 2147, 2010.
- [23] K. Glover, J. Strang, and A. Lubansky, “Characterising the effect of geometry on a microchamber for producing controlled concentration gradients,” *Chemical Engineering Science*, vol. 117, pp. 389–395, Sep. 2014.
- [24] S. Paliwal, P. A. Iglesias, K. Campbell, Z. Hilioti, A. Groisman, and A. Levchenko, “MAPK-mediated bimodal gene expression and adaptive gradient sensing in yeast,” *Nature*, vol. 446, no. 7131, pp. 46–51, Mar. 2007.
- [25] E. Cimetta *et al.*, “Microfluidic device generating stable concentration gradients for long term cell culture: application to Wnt3a regulation of β -catenin signaling,” *Lab on a Chip*, vol. 10, no. 23, p. 3277, 2010.
- [26] T. S. Kaminski, S. Jakiela, M. A. Czekalska, W. Postek, and P. Garstecki, “Automated generation of libraries of nL droplets,” *Lab on a Chip*, vol. 12, no. 20, p. 3995, 2012.
- [27] E. Fradet, C. McDougall, P. Abbyad, R. Dangla, D. McGloin, and C. N. Baroud, “Combining rails and anchors with laser forcing for selective manipulation within 2D droplet arrays,” *Lab on a Chip*, vol. 11, no. 24, p. 4228, 2011.
- [28] P. Laval, N. Lisai, J.-B. Salmon, and M. Joanicot, “A microfluidic device based on droplet storage for screening solubility diagrams,” *Lab on a Chip*, vol. 7, no. 7, p. 829, 2007.
- [29] J. L. Plawsky, *Transport phenomena fundamentals*. New York: Marcel Dekker, 2001.
- [30] F. P. Incropera and F. P. Incropera, Eds., *Fundamentals of heat and mass transfer*, 6th ed. Hoboken, NJ: John Wiley, 2007.
- [31] M. Morel, J.-C. Galas, M. Dahan, and V. Studer, “Concentration landscape generators for shear free dynamic chemical stimulation,” *Lab on a Chip*, vol. 12, no. 7, p. 1340, 2012.
- [32] D. Huh *et al.*, “Gravity-Driven Microfluidic Particle Sorting Device with Hydrodynamic Separation Amplification,” *Analytical Chemistry*, vol. 79, no. 4, pp. 1369–1376, Feb. 2007.
- [33] D. Di Carlo, “Inertial microfluidics,” *Lab on a Chip*, vol. 9, no. 21, p. 3038, 2009.
- [34] “What is Reynolds Number - Definition of Reynolds Number,” *Nuclear Power*. [Online]. Available: <https://www.nuclear-power.net/nuclear-engineering/fluid-dynamics/reynolds-number/>. [Accessed: 26-Sep-2018].
- [35] K. Lee *et al.*, “Generalized serial dilution module for monotonic and arbitrary microfluidic gradient generators,” *Lab Chip*, vol. 9, no. 5, pp. 709–717, 2009.
- [36] “What Is Diffusion?,” 08-Oct-2018. [Online]. Available: <https://www.comsol.com/multiphysics/what-is-diffusion>. [Accessed: 08-Oct-2018].

- [37] P. Atkins and J. De Paula, *Thermodynamics and kinetics*. New York: W.H. Freeman and Co., 2005.
- [38] "Diffusion Equation: Fick's Laws of Diffusion." [Online]. Available: <https://www.comsol.com/multiphysics/diffusion-equation>. [Accessed: 15-Nov-2018].
- [39] "What Is Convection?" [Online]. Available: <https://www.comsol.com/multiphysics/what-is-convection>. [Accessed: 15-Oct-2018].
- [40] Z. Xu, X. Huang, P. Wang, H. Wang, and D. A. Weitz, "Optimization and development of a universal flow-based microfluidic gradient generator," *Microfluidics and Nanofluidics*, vol. 20, no. 6, Jun. 2016.
- [41] "Data-sheet-OSTEMER-322-Crystal-Clear-v5.pdf." .
- [42] D. Sticker, M. Rothbauer, S. Lechner, M.-T. Hehenberger, and P. Ertl, "Multi-layered, membrane-integrated microfluidics based on replica molding of a thiol-ene epoxy thermoset for organ-on-a-chip applications," *Lab on a Chip*, vol. 15, no. 24, pp. 4542–4554, 2015.
- [43] "PDMS: A review," *Elveflow*. .
- [44] Smokefoot, *English: improved image of polydimethylsiloxane*. 2012.
- [45] W.-I. Wu, K. N. Sask, J. L. Brash, and P. R. Selvaganapathy, "Polyurethane-based microfluidic devices for blood contacting applications," *Lab on a Chip*, vol. 12, no. 5, p. 960, 2012.
- [46] A. Piruska *et al.*, "The autofluorescence of plastic materials and chips measured under laser irradiation," *Lab on a Chip*, vol. 5, no. 12, p. 1348, 2005.
- [47] J. C. McDonald *et al.*, "Fabrication of microfluidic systems in poly(dimethylsiloxane)," *Electrophoresis*, vol. 21, no. 1, pp. 27–40, Jan. 2000.
- [48] "f6377pis.pdf." .
- [49] "F6377-BULK_____SIAL_____.pdf." .
- [50] J. Banks, Ed., *Discrete-event system simulation*, 3rd ed. Upper Saddle River, NJ: Prentice Hall, 2001.
- [51] B. Andersson, Ed., *Computational fluid dynamics for engineers*. Cambridge ; New York: Cambridge University Press, 2012.
- [52] "Meshing -- CFD-Wiki, the free CFD reference." [Online]. Available: <https://www.cfd-online.com/Wiki/Meshing>. [Accessed: 29-Oct-2018].
- [53] "What is a Mesh? — SimScale Documentation." [Online]. Available: <https://www.simscale.com/docs/content/simwiki/preprocessing/whatisamesh.html>. [Accessed: 29-Oct-2018].
- [54] "geoandgrid.pdf." .
- [55] "GAMBIT Software." [Online]. Available: <https://www.poweronline.com/doc/gambit-software-0001>. [Accessed: 03-Nov-2018].
- [56] "CFD-gambit 2.2 tutorial.pdf." .
- [57] Z. Hu, X. Chen, and L. Wang, "Design and Fabrication of Concentration-Gradient Generators with Two and Three Inlets in Microfluidic Chips," *Chemical Engineering & Technology*, vol. 41, no. 3, pp. 489–495, Mar. 2018.
- [58] D. Irimia, D. A. Geba, and M. Toner, "Universal Microfluidic Gradient Generator," *Analytical Chemistry*, vol. 78, no. 10, pp. 3472–3477, May 2006.